

The Faults in our State

An investigation of earthquakes in Maryland

Yuval Ravinsky-Gray

11/25/2024

Advisor: Vedran Lekic
GEOL394: Senior Thesis



ABSTRACT

Small earthquakes occur on average once a year in Maryland and are rarely studied in detail to determine focal mechanisms, mostly because of data limitations and incomplete information about subsurface structure. Investigating seismicity in Maryland can help to properly assess seismic hazards, reveal valuable information about local geology and stress, and provide insight for other fields using sparse data, such as planetary seismology. It was hypothesized that earthquakes occurred on reverse faults consistent with the SW-NE trend of the Atlantic Fall line, consistent with mapped fault systems in Virginia that trace back to Paleozoic compression and Mesozoic extension processes.

This research seeks to determine whether robust moment tensor solutions can be determined for small earthquakes in Maryland given the sparsity of available waveform data and the low signal-to-noise ratio in some of the data. If stable solutions are possible, then we also seek to determine if a pattern in the solutions supports the presence of a primary fault system on which slip occurs.

We focus on moment tensor inversion of a 2.6 magnitude earthquake that occurred on June, 25th, 2021 in Baltimore, Maryland. A one-dimensional seismic velocity structure was used for the inversion. The range of likely models was constrained by comparing local velocity models with the results of a surface wave dispersion inversion. A depth of 9 km was selected, as this maximized the variance reduction in the inversion.

Results indicate that stable moment tensor solution can be found. Moment tensors for the 6/25/2021 Baltimore earthquake were produced using 3 different local 1-dimensional velocity models and one “test” model, designed to be constrained within the range of likely models. The resulting focal mechanisms were well within the threshold for statistical similarity and showed a maximum difference in strike, dip, and rake of 15° or less. The two fault plane solutions were (strike = 148°, dip = 70°, rake = -74°) and (strike = 281°, 28°, -137°), indicating a dominant normal faulting mechanism. The first of these solutions was interpreted as the true solution based on considerations of local geology.

PLAIN LANGUAGE ABSTRACT

Small earthquakes occur on average once a year in Maryland and are almost never studied. Investigating earthquakes in Maryland can give a better picture of real earthquake hazards for the mid-Atlantic region. This knowledge can also help explain why earthquakes occur in regions far from tectonic plate boundaries. In addition, by studying these earthquakes, scientists can learn about the local structure of the Earth and geological history.

This research examines a 2.6 magnitude earthquake that occurred in 2021 in Baltimore, Maryland. The goal is to determine the orientation of the fault on which this earthquake occurred, as well as the fault motion based on the available seismic data. The author hypothesized that the fault would be oriented NE-SW and that the fault motion was driven by compressive forces. This hypothesis was based on the orientation of other known faults in Virginia and the behavior of a few previously studied earthquakes. However, the research must first answer whether locating faults in Maryland is even possible, given that there are very few local stations that record earthquake data, and this data is not always of the best quality.

A two-part process was used to try to reconstruct the fault motion. The first involved finding models of the local seismic velocity structure. These models tell us how fast earthquake waves travel through the ground at different depths. Velocity models produced by previous studies were compiled and compared. These models were then supplemented by a study that used data from surface waves (seismic waves that travel near the surface) to reconstruct a more exact velocity structure. Four different possible models were used in the second part: the inversion. These models were used to produce “synthetic” i.e. idealized seismograms using a mathematical algorithm. The synthetic seismograms were used along with the real seismogram data in a mathematical operation called “moment tensor inversion” that finds the fault motion which best fits the data. In order to determine whether the fault motion can be reconstructed, the research compared the results of the inversion for all four models.

The four models produced consistent fault solutions, indicating that moment tensor inversion can successfully recover the orientation of faults for small earthquakes in Maryland. Contrary to the author’s initial hypothesis, the results suggest that the fault for the 6/25/21 Baltimore earthquake is oriented SE-NW and that the fault motion is driven by tension.

Table of Contents

| | |
|--|-----------|
| <i>ABSTRACT</i> | 1 |
| <i>PLAIN LANGUAGE ABSTRACT</i> | 1 |
| <i>INTRODUCTION & MOTIVATION</i> | 5 |
| <i>BACKGROUND</i> | 7 |
| <i>SEISMICITY IN THE EASTERN UNITED STATES</i> | 7 |
| <i>THE STRESS FIELD</i> | 10 |
| <i>FOCAL MECHANISMS</i> | 10 |
| <i>GEOLOGICAL MAPS</i> | 13 |
| <i>HYPOTHESES</i> | 15 |
| <i>METHOD OF ANALYSIS</i> | 17 |
| <i>MATHEMATICAL BACKGROUND</i> | 17 |
| <i>THE FORWARD PROBLEM</i> | 18 |
| <i>THE INVERSE PROBLEM</i> | 19 |
| <i>ANALYSIS OF UNCERTAINTY</i> | 21 |
| <i>PRESENTATION OF DATA</i> | 24 |
| <i>DISCUSSION OF RESULTS</i> | 34 |
| <i>SUGGESTIONS FOR FUTURE WORK</i> | 35 |
| <i>CONCLUSION AND BROADER IMPLICATIONS</i> | 37 |
| <i>ACKNOWLEDGEMENTS</i> | 37 |
| <i>BIBLIOGRAPHY</i> | 37 |
| <i>APPENDIX A: Velocity models referenced</i> | 43 |
| <i>APPENDIX B: Code for moment tensor inversion</i> | 46 |

Table of Tables and Figures

| | |
|---|----|
| Table 1: Basic information for studied earthquake.. | 13 |
| Table 2: Stations used for inversion | 21 |
| Table 3: Local models used to constrain the velocity model | 24 |
| Figure 1: Earthquakes in Maryland..... | 5 |
| Figure 2: U.S. National seismic hazard maps..... | 7 |
| Figure 3: Seismicity in the Eastern United States..... | 8 |
| Figure 4: Figures from Soto-Cordero et al. (2018)..... | 9 |
| Figure 5: Stress inversion by Levandowski et al. (2018)..... | 10 |
| Figure 6: Explanation of Focal Mechanisms | 11 |
| Figure 7: A Hudson plot | 12 |
| Figure 8: Known focal mechanisms for the mid-Atlantic states | 12 |
| Figure 9: Geological maps of Baltimore..... | 13 |
| Figure 10: Fault systems in the DMV region | 14 |
| Figure 11: Example reverse faulting moment tensor aligned with the Fall Line | 16 |
| Figure 12: Stations used in the inversion | 20 |
| Figure 13: histogram of random moment tensor angles | 23 |
| Figure 14: Graphical explanation of uncertainty analysis..... | 24 |
| Figure 15: Steps of the forward problem | 25 |
| Figure 16: Surface Wave dispersion data | 26 |
| Figure 17: Variance reduction vs. Depth for 5 different models..... | 28 |
| Figure 18: Data vs inversion waveforms for Chapman (2013) model | 29 |
| Figure 19: Data vs inversion waveforms for Nyblade & Homman (2016) model | 30 |
| Figure 20: Data vs inversion waveforms for Munsey & Bollinger (1985) model..... | 31 |
| Figure 21: Data vs inversion waveforms for Test Model | 32 |
| Figure 22: Inversion results for the four models | 33 |
| Figure 23: Full moment tensor information | 34 |

INTRODUCTION & MOTIVATION

Neither Maryland nor the entire East Coast is generally thought of as an active seismic zone. Nevertheless, small (up to 3.6 magnitude) earthquakes occur about once a year. While some events recorded by seismic stations are almost certainly mining blasts or military ordinance tests, many do not show a clear connection to human activity. **Figure 1A** displays all seismic events recorded in Maryland and the surrounding region since 1965. Data are from the International Seismological Center (ISC) database. Quarries, mines, and military testing sites, identified by the author using Google Earth and Google Maps, are shown as well. In **Figure 1B** all seismic events within 5 km of a possible human source have been removed. The remaining events are likely earthquakes. The vast majority of them occur within the Piedmont province.

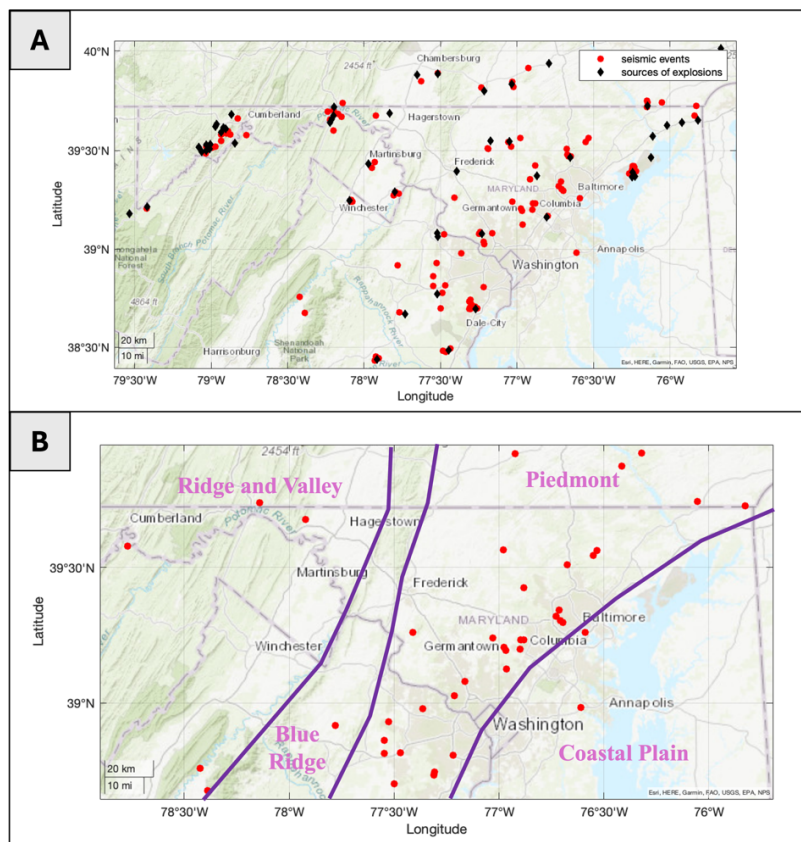


Figure 1: Earthquakes in Maryland. A) Seismic events (red circles) and sources of manmade explosions (black diamonds) in Maryland and surrounding region are plotted. Sources of explosions include quarries, coal mines, and military testing sites. Seismic data is from the ISC database. Quarries and other explosive sources were located using Google Earth. B) Probable earthquakes: all seismic events within 5 km of a source of explosions have been removed. Events in Western Maryland appear to be associated with coal mining. None remain west of Cumberland after the filtering process. Physiographic province boundaries are shown in purple. Almost all likely natural events fall within the Piedmont.

Very little is known about the causes of earthquakes in Maryland. Asked to comment on the origin of an earthquake in Columbia, MD, on April 1st, 1993, Dr. Leonard Seeber of the Lamont-Doherty Earth Observatory suggested that the seismic activity was related to a nearby dike and might be connected to a 4.0 event in Lancaster PA (New York Times, 1993). However, we can find no systematic study to test speculation. The only event that has been studied is the 3.6 Mw 2010 Germantown earthquake. A moment tensor was calculated by the USGS. Source parameters and stress change were calculated by Viegas (2012) and were examined in connection with the 2011 Mineral, VA earthquake by University of Maryland PhD student Lisa Schreier Walsh in her dissertation (Walsh, 2013). Neither Viegas nor Walsh attempt to connect the Germantown event to a specific fault, nor has anyone studied the causes of the stress driving these earthquakes.

The question arises: why should we study these earthquakes? No Maryland earthquake above a 3.6 magnitude has been recorded, and none have resulted in deaths or significant property damage. The answer is twofold: 1. Studying even small seismicity can inform seismic hazard assessment; 2. Characterizing seismic deformation in a region can provide clues into the stress state and help us understand why intraplate earthquakes occur where and when they do.

Assessment of seismic hazards is highly dependent on previous seismic records (Soto-Cordero et al., 2018). Since instrumental earthquake records only go back about 50 years and records of ground-shaking in the United States only go back four hundred years, there is a significant possibility for surprisingly strong events to occur. In China, where records extend back to about 3000 years ago, regions of low seismicity lasting 300-500 years have been interrupted by pulses of strong activity (Yang & Aggarwal, 1981). Allen (1975) warned that “the very short historic record in North America should, therefore, be used with extreme caution in estimating possible future seismic activity.”

For example, although the 2011 Mineral, Virginia Earthquake occurred in an area known to be seismically active, the 5.8 Mw quake released over an order of magnitude more energy than was anticipated by hazard assessments (Moschetti and Haller, 2014) and caused over \$80 Million in damage. The ground shaking exceeded safety limits for the nearby North Anna, VA, nuclear power plant, causing a temporary shutdown (Walsh, 2013). As a result, the national seismic hazard model was updated to increase the likelihood of strong shaking in the area (**Figure 2**). Maryland is home to several vulnerable structures, namely the Calvert Cliffs nuclear power plant and the Conowingo hydroelectric dam on the Susquehanna River. Failure of either of these would have catastrophic consequences. To add to the problem, faults in Maryland are poorly mapped. The existence of some is debated (Drake, 1998), while others may be unmapped.

Another compelling reason to study Maryland earthquakes is the breadth of unsolved geological problems connected to this seemingly picayune issue. Causes of intraplate earthquakes are poorly understood, and a number of triggering mechanisms have been suggested including tectonic forces such as ridge push and basal drag, crustal collapse due to gravity, isostatic adjustment from erosion or glacial rebound, variations in crustal density or strength, upper mantle convection anomalies (Levandowski et al., 2018), stress changes from distant earthquakes (Hough & Bilham, 2006) and a multitude of local causes including human action. Likewise, the causes of the stress field in the Eastern United States are not clear (Lundstern and Zoback, 2020). The detailed study of earthquakes in this region may contribute to answering these questions, which have relevance to global tectonic processes. Additionally, a complex history of orogeny and rifting over the past billion years is imprinted in networks of faults and

igneous structures throughout the Eastern United States. Confirmation of existing faults or the discovery of new faults will contribute to knowledge of Appalachian tectonic history.

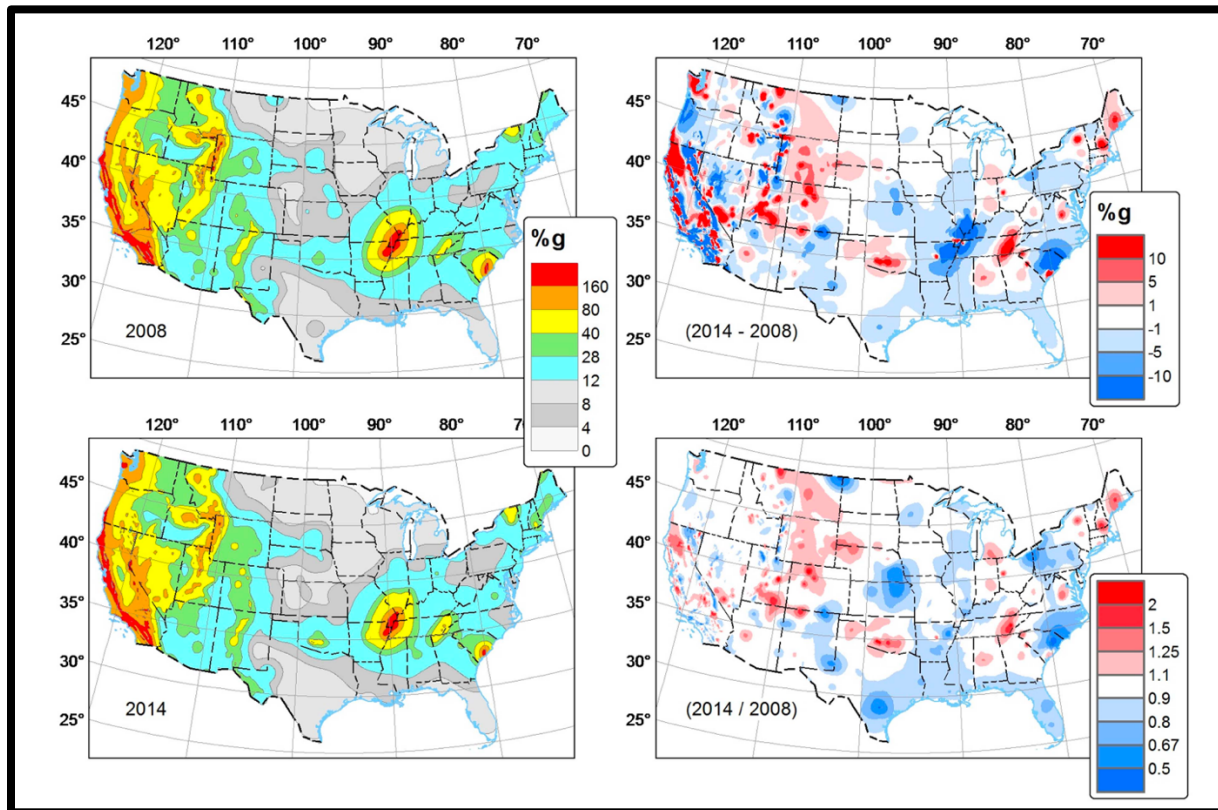


Figure 2: U.S. National seismic hazard maps for 2008 (top left) and 2014 (bottom left) at 5 Hz acceleration. The colors on the left indicate the amount of 5 Hz shaking that there is a 2% chance of exceeding in 50 years. Also shown are difference (2014-2008, top right) and ratio (2014/2008, bottom right) maps. Colors on the right represent the difference in the hazard assessments, red for increased hazard and blue for decreased hazard. Figure from Peterson et al. (2014). Note the increase in seismic hazard from 2008 to 2014 near Mineral, Virginia after the 2011 earthquake. Also noteworthy are increased seismic hazards in Tennessee and New England. The change illustrates how hazard assessment depends on earthquake history.

BACKGROUND

SEISMICITY IN THE EASTERN UNITED STATES

Earthquakes in Maryland do not occur in isolation but are part of a band of seismicity that runs broadly parallel to the Appalachian Mountains as seen in **Figure 3**. While this band coincides highly with the Southern Appalachian Mountains (the Eastern Tennessee seismic zone) in the southern Appalachians, in the middle and northern Appalachians the concentration of earthquakes is much higher east of the mountains. In the Mid-Atlantic states from Virginia to New York, this geographic concentration strongly follows the Piedmont province, or the Fall

Line, boundary between this province and the Coastal Plain. If we look at earthquakes of all magnitudes, there is a minor trend that continues along the Piedmont/Coastal Plain boundary all the way to Georgia (**Figure 3B**).

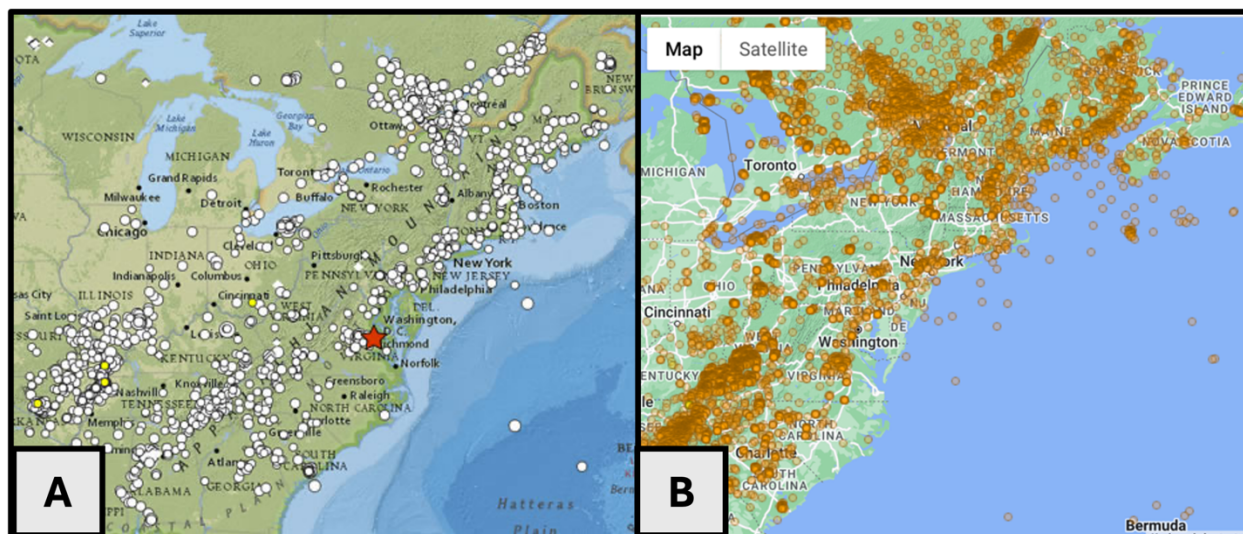


Figure 3: *Seismicity in the Eastern United States. A) Earthquakes in the Eastern U.S. from 1973 to February 12, 2015. The red star marks the epicenter of the August 2011 Mineral VA earthquake. Caption and image from USGS earthquake hazards program (2019). B) Map of all earthquakes in the pictured region since 1974 that are recorded in the IRIS database. More events with lower magnitudes are included in this dataset. The trend of Piedmont earthquakes appears to continue to South Carolina and Georgia.*

In the Mid-Atlantic states, seismicity is commonly grouped into seismic zones. Soto-Cordero et al. (2018) performed a cluster analysis of the surface locations of earthquakes in the mid-Atlantic and northeastern states and identified three “hot spots” of activity (**Figure 4A**). They labeled these the Central Virginia Seismic Zone (CVSZ), the site of the 2011 Mineral, Virginia earthquake; the Reading-Lancaster Seismic Zone (RLSZ), in southeastern Pennsylvania; and the Ramapo Seismic Zone (RSZ), the site of the 2024 4.8 M_w earthquake in New Jersey. While Maryland and Northern Virginia are in a gap between these clusters, the authors note that statistically this region is not a gap: earthquakes clearly occur here, even though it is not classified as cluster.

The authors also examined the correlation of seismicity in the Mid-Atlantic United States with crustal structure. They analyzed a data set of 581 earthquakes including both recent events and those occurring before measurement was available. The data were rigorously “declustered” to remove aftershocks and anthropogenic events. Crustal structure was determined along four seismic lines deployed at various latitudes across the Eastern United States from Virginia to New England. The results indicated that along most of the Appalachian region the crust rapidly thickens westward across the Piedmont province (gaining around 1 km depth per every 2 km distance in places) and tends to level out near the Valley and Ridge province (**Figure 4B**). Earthquakes from the data set clustered around this strong Moho gradient below the Piedmont.

The authors suggest that the steep crustal gradient acts as a “buttress,” focusing stress. However, they note that with the relatively consistent Moho gradient along the Appalachians, a more uniform band of seismicity would be expected. They propose that stress may become

temporarily concentrated in local faults and shift over time, resulting in a uniform distribution of earthquakes across the Piedmont over long periods. This would imply that seismic hazard maps need to be updated and that an earthquake of similar magnitude to the Mineral, Virginia event could occur anywhere in the Piedmont.

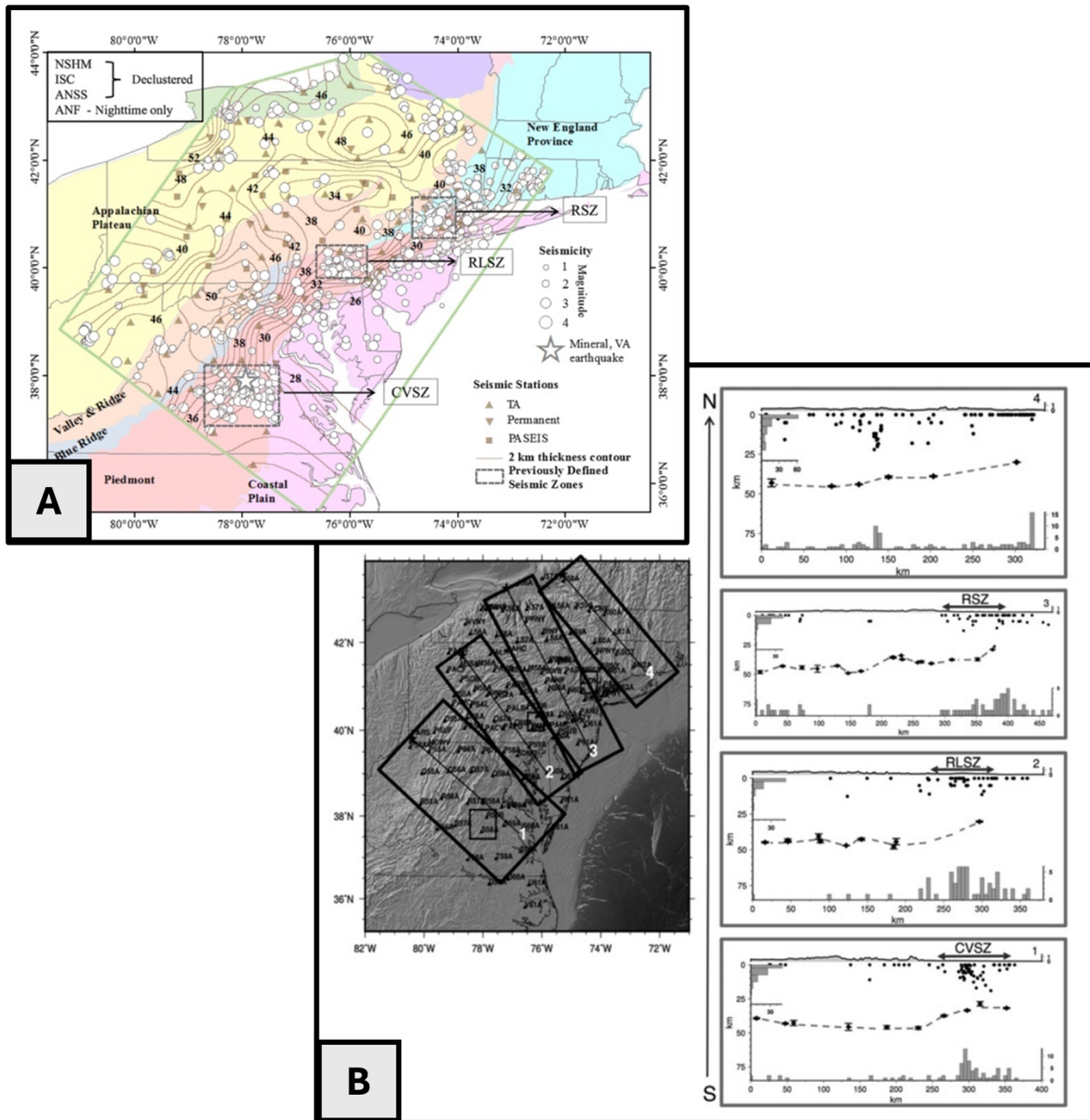


Figure 4: Figures from Soto-Cordero et al. (2018) A) Earthquakes in the Mid-Atlantic states. Boxes indicate seismic “hot spots” identified by the authors. Colors indicate physiographic provinces, while contour lines show changes in crustal thickness. B) Left: the four seismic lines deployed by the authors to determine crustal structure. Right: Moho depth measurements are indicated by diamonds connected by a dashed line representing the Moho profile. Dots refer to individual earthquakes. Histograms on the x and y axes show the concentration of earthquakes by distance along the line and by depth. Earthquakes are concentrated along the Piedmont province where the Moho gradient tends to steepen.

THE STRESS FIELD

It is not clear how earthquakes in Maryland relate to the stress field in eastern North America or whether there may be a local stress field that controls slip along faults. Many publications (Zoback and Zoback, Heidbach et al., 2018; Lundstern and Zoback, 2020) show a general trend of ENE-WSW compressional stress in the eastern United States. A stress inversion by Levandowski et al. (2018) agrees with this trend but finds the maximum compressional stress axis to be closer to E-W in some parts of Maryland and Virginia (**Figure 5**). Finding fault plane solutions for Maryland earthquakes can help address this discrepancy.

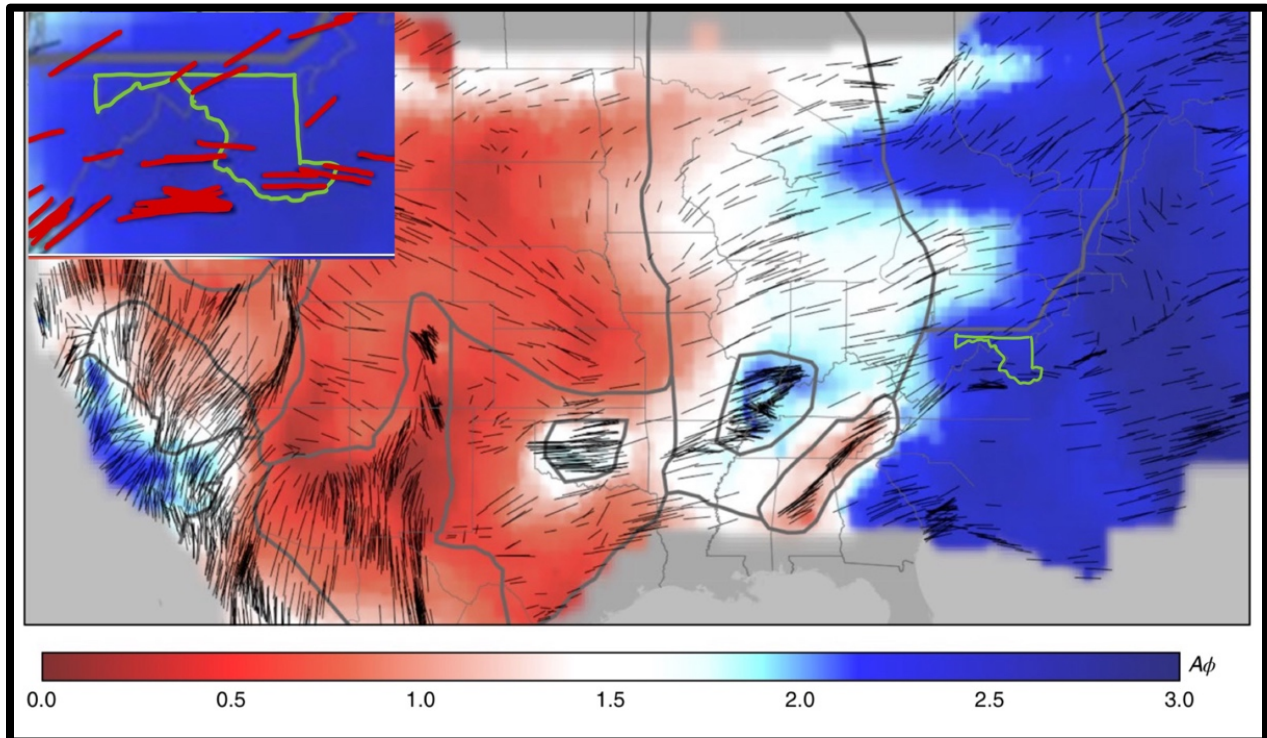


Figure 5: Stress inversion by Levandowski et al. (2018). Blue areas are in compression, white areas are in a strike-slip regime, and red areas are in tension. Variations on the color bar indicate gradations between these extremes. Maryland has been highlighted in green and is shown in the top left inset with stresses in red for visual clarity.

FOCAL MECHANISMS

This research seeks to identify the type of fault motion responsible for Maryland earthquakes. This is done through a process known as moment tensor inversion, described in detail in the Methods section. A moment tensor is a matrix encoding of the motion at a fault source, or fault plane solution i.e. the strike, dip, and rake. The information from this matrix is often plotted using a focal mechanism or “beachball,” a stereographic projection of first motions at the source. **Figure 6** presents basic information about focal mechanisms. Note that focal

mechanisms always have two possible fault plane solutions. The borders of the light and dark areas represent the 2 fault planes. The correct one is chosen from knowledge of local geology.

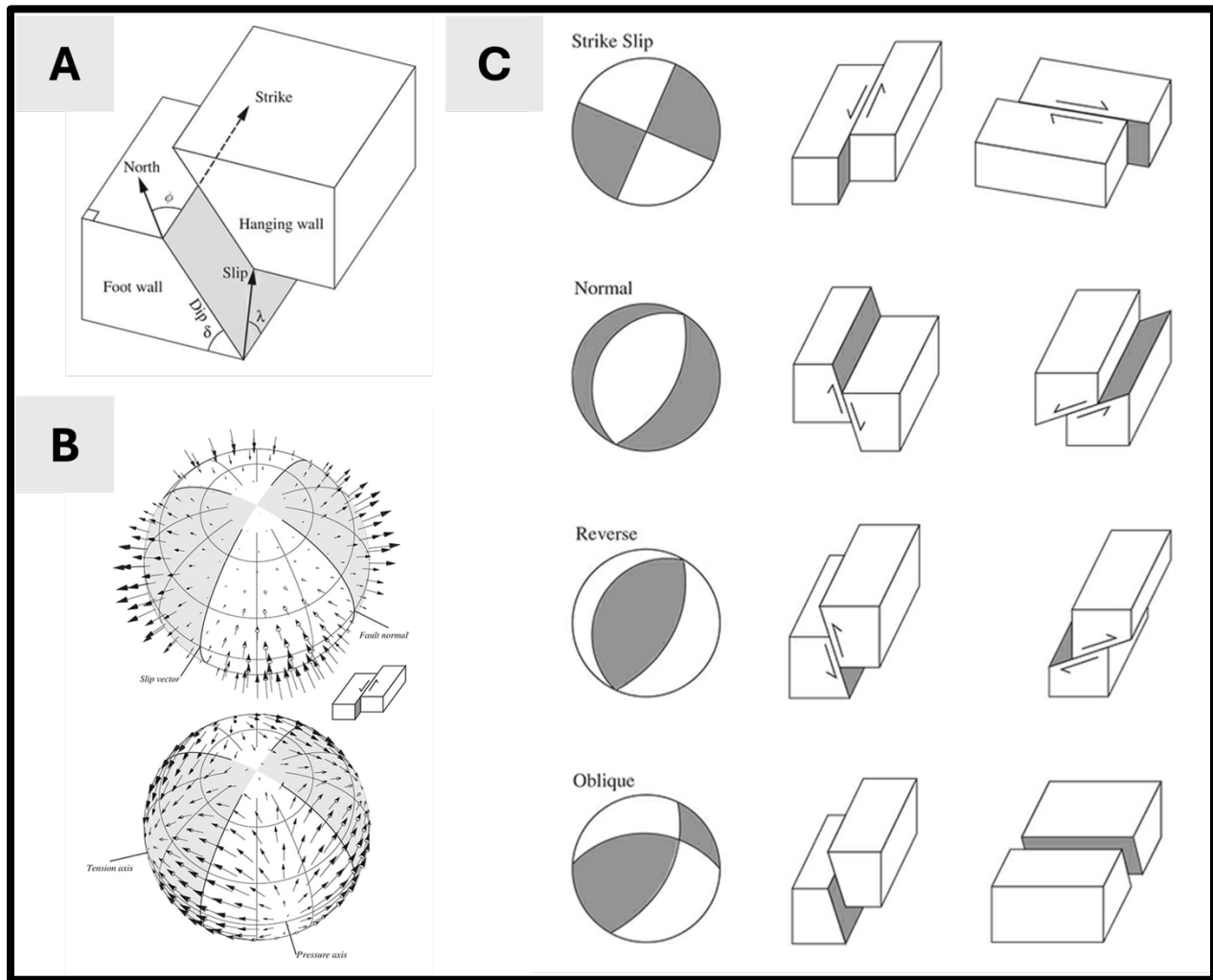


Figure 6: Explanation of Focal Mechanisms. Figures are from Shearer (2019) A) Diagram showing fault plane solution parameters: strike, dip, and rake (slip). B) First motions for P (top) and S (bottom) waves. C) Basic focal mechanisms and their 2 fault plane solutions.

Moment tensors can include components that reflect motion other than pure slip along a fault. These are often removed from the moment tensor by a matrix operation known as moment tensor decomposition. The isotropic component representing explosive or implosive motion is removed first. The modified moment tensor, called the deviatoric moment tensor, is commonly used to make beachball plots. The pure fault slip element is known as a double couple and can be isolated from the deviatoric moment tensor by finding the “best double couple” i.e. the decomposition that maximizes the double couple component. The remaining matrix, known as a Compensated Linear Vector Dipole or CLVD can represent expansion or contraction of a crack. An earthquake moment tensor should have a dominant double couple component: high isotropic and CLVD components may be indicative of modeling error. A Hudson plot (**Figure 7**) can be used to visualize the strength of each of the non-double couple components. Percent isotropic

component is plotted on the vertical axis, while percent CLVD is plotted on the horizontal axis. A pure double couple is located at the origin. Moment tensor solutions for earthquakes sometimes contain significant non-double couple components. For example, the USGS solution to the 2024 Tewksbury, NJ earthquake is only 58% double couple (USGS, 2024).

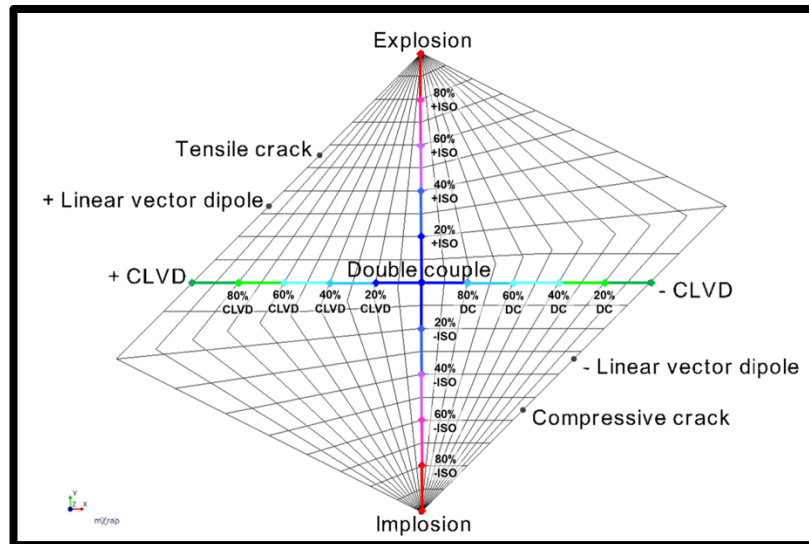


Figure 7: A Hudson plot. Used for comparing the components of a moment tensor and identifying the type of source motion.

Focal mechanisms have been found for a few earthquakes in the mid-Atlantic states (**Figure 8**). These include the largest earthquake in Maryland, the 3.4 - 3.6 magnitude earthquake near Germantown in 2010 (USGS, 2010), as well as the 2011 Mineral, Virginia earthquake (USGS, 2011), the November 2017 4.2 Mw Delaware, a 1994 event near Reading, PA (Kim et al., 2018), and the April 2024 4.8 Mw New Jersey event (USGS, 2024). All of these focal mechanisms show reverse faulting consistent with the stress map produced by Levandowski et al. (2018) (**Figure 5**).

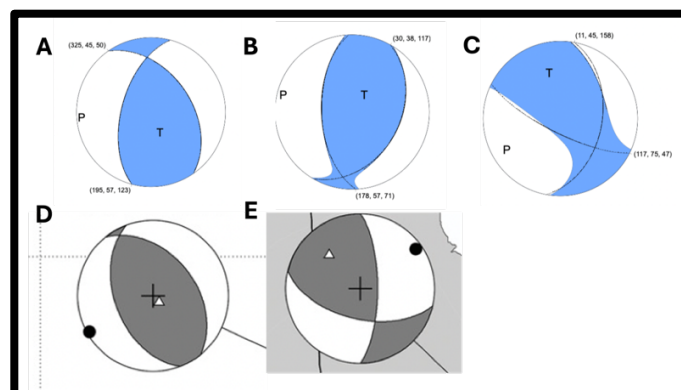


Figure 8: Known focal mechanisms for the mid-Atlantic states A) Germantown, MD, 2010 B) Mineral, VA, 2011. C) Tewksbury, NJ, 2024 (USGS) D) Reading, PA, 1994. E) Dover, DE, 2017 (Kim et al., 2018)

GEOLOGICAL MAPS

This research investigates a single earthquake that occurred on June 25th, 2021, near Leakin Park in Baltimore. Basic information for the earthquake studied in this research is displayed in **Table 1**. This earthquake is notable because it is one of four Maryland earthquakes that occurred in 2021, three of them within a few kilometers of each other in Baltimore. The 6/25/21 event is suspected to have triggered the other two nearby quakes, which occurred two days and one month after respectively.

| Location | Date | Time (UTC) | Lat | Long | Mag | Depth (km) |
|-----------|------------|-------------|---------|----------|-----|------------|
| Baltimore | 2021-06-25 | 19:40:45.27 | 39.3046 | -76.7089 | 2.6 | 2.5 |

Table 1: Basic information for studied earthquake. Data is from the International Seismological Center (ISC) database.

A geological map of Baltimore City by Crowley et al. (1976) shows that all three 2021 Baltimore earthquake epicenters are located on the igneous and metamorphic Laurel Belt, which is bounded by thrust faults to the North and West. Just north of the Laurel Belt, there is also a system of normal faults. See **Figure 9A** for details. Any of these mapped fault systems might have been the location for the 6/25/21 earthquake or its likely aftershocks. Geological units are mapped more clearly in a 7.5-minute quadrangle map of West Baltimore by Crowley and Reinhardt (1979), seen in **Figure 9B**. Some of the contacts might represent unmapped faults, one of which might be the source of the earthquakes.

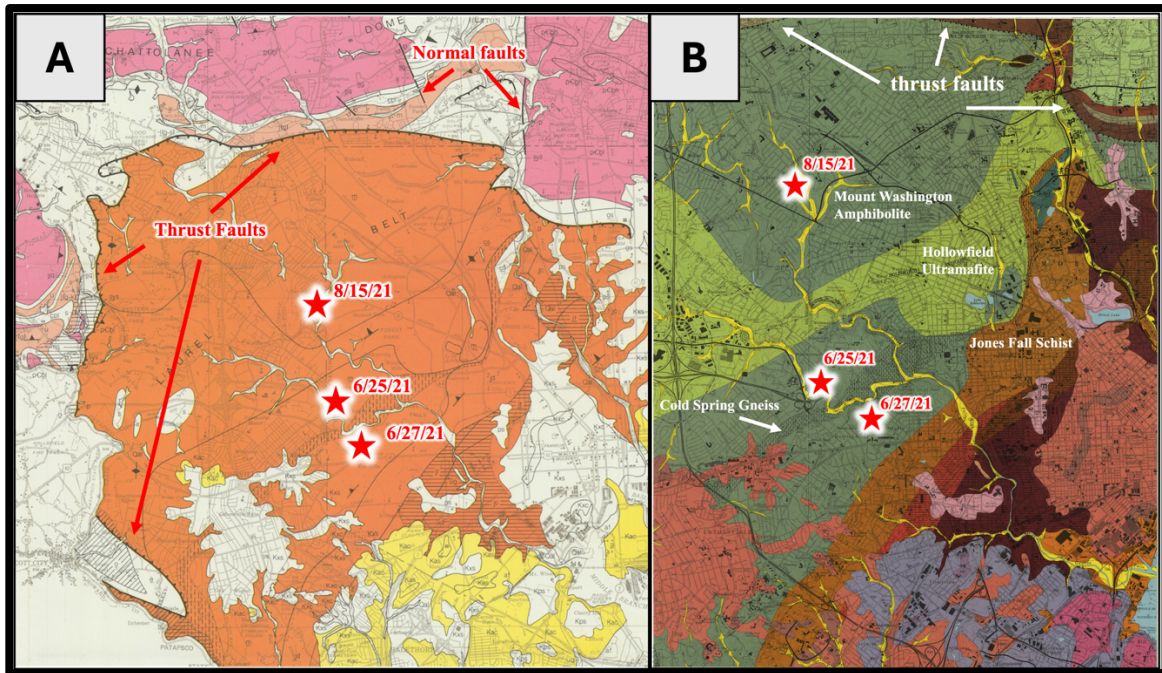


Figure 9: Geological maps of Baltimore. A) From Crowley et al. (1976). The studied earthquake and two possible aftershocks are shown as red stars. The Laurel Belt, depicted in orange, is bounded by thrust faults. A system of normal faults also lies to the North. B) From the geological map of the West Baltimore quadrangle by Crowley and Reinhardt (1979). Nearby geological units and mapped faults and labeled.

The 2011 Mineral, VA, earthquake occurred along a system of faults running NE-SW parallel to the trend of the Appalachian mountains and parallel to the trend of the Piedmont and Fall Line in Northern Virginia, DC, and Maryland. These are interpreted as bounding accreted terranes thrust onto Laurentia during the Taconic, Acadian, and Alleghanian orogenies (Horton et al, 2015). Further faults are also associated with Mesozoic extension (Walsh, 2013). These faults and terranes are seen in **Figure 10**. Walsh (2013) suggests that the 90-degree bend in the Potomac River that causes it to run along the Fall Line for about 50 km may be influenced by the nearby Stafford Fault System. She also notes that structural features and lithological contacts appear to coincide with major knickzones along the Potomac and Susquehanna Rivers at the Fall Line, suggesting an association of this feature with tectonic activity. Similar systems of NE-SW running faults have been mapped near Columbia, MD, by Drake (1993) and in Baltimore City north and east of the section shown in **Figure 9** (Crowley et al.,1976). More such thrust faults may lie hidden below the surface closer to the listed epicenter.

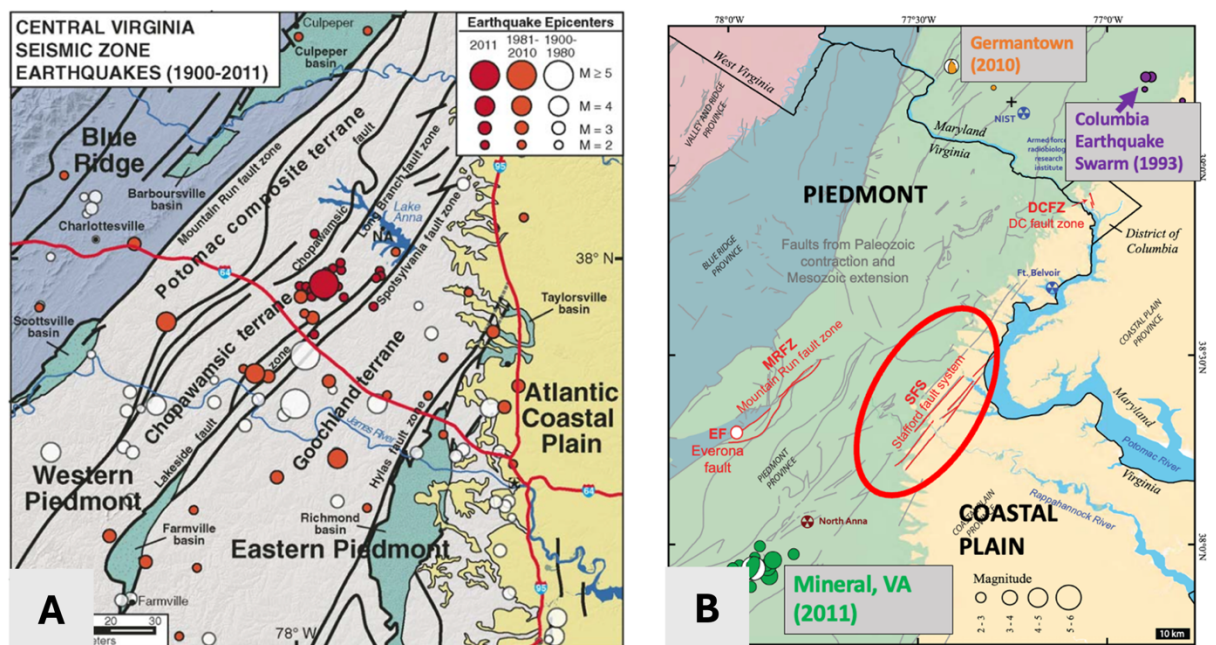


Figure 10: Fault systems in the DMV region A) Map from Horton et al. (2015) showing NE-SW running faults and associated terranes in the CVSZ. The Fall Line coincides with these faults to the Northeast as shown in B. The red circles represent the 2011 Mineral earthquake and associated aftershocks. B) Map from Walsh (2013) showing fault systems in Virginia, DC, and Maryland and seismic events. Some captions have been enlarged for clarity. The Mineral Virginia earthquake and aftershocks are shown with a focal mechanism in green. The 2010 Germantown earthquake with one aftershock is shown with focal mechanism in orange. The 1993 swarm of earthquakes in Columbia is shown in purple. Walsh (2013) notes that the 90-degree curve of the Potomac River may be influenced by the Stafford Fault System, which runs along the Fall Line. Radiation hazard signs mark the locations of present and former nuclear reactors.

HYPOTHESES

Moment tensor inversion of small earthquakes in Maryland presents numerous challenges. First of all, the local seismic station network is sparse, meaning that only a few local stations pick up a usable signal. A dense seismic network is helpful because the inversion problem has many more possible solutions (the problem is less constrained) when only a few waveforms are sampled. Secondly, given that the earthquakes are small (mostly magnitude below 2.7), the signal is attenuated over longer distances, meaning that so called teleseismic stations cannot pick them up. This presents two problems: 1. it further reduces the number of stations available and 2. it means that the seismic waves do not travel as far, so they do not reach as deep into the crust and mantle. This means that general Earth models such as PREM cannot be used, and that problem is more sensitive to variations in the seismic velocity structure of the crust and upper mantle. This research employs a 1-dimensional, homogeneous, flat layer model, and differences between model and reality can be significant.

In order to get around problems from crustal velocity variation, it is common practice to use very high period (low frequency) energy for inversions, since low frequencies are not as sensitive to these velocity differences. However, in the mid-Atlantic Piedmont region, there is very high seismic noise at low frequencies. Addressing this issue necessarily involves finding a “golden zone” in which the signal-to-noise ratio (SNR) is high enough to avoid interference and the frequency is low enough that the inversion can match a significant portion of the waveform. With these difficulties in mind, the following primary hypothesis is adopted:

NULL HYPOTHESIS 1:

Moment tensor inversion using the selected tools is unable to produce a stable focal mechanism for the selected Maryland earthquake.

These tools are as follows: Pyprop8 (a lightweight Python package for calculating synthetic seismograms), waveform and first arrival data for local stations available on the International Seismological Center (ISC) and EarthScope Wilber3 public databases, surface wave dispersion data from the USArray seismic network, and a Python program for transdimensional Bayesian inversion of surface wave dispersion data.

Null hypothesis 1 is supported if the inversion is so sensitive to error in the velocity model that all results fall within the range of uncertainty and no conclusions can be made. Uncertainty is quantified by the maximum normalized moment tensor angle between results found using different reasonable velocity models, as discussed in the Uncertainty Analysis section. The threshold for accepting the alternative hypothesis is an angle of 0.21. At or below this value, there is approximately a 98% probability that the moment tensor similarity is not due to random chance. Additionally, since finding fault plane solutions is a major goal of this research, the maximum uncertainty in strike, dip, or rake must not be below 20°.

ALTERNATIVE HYPOTHESIS 1:

Moment tensor inversion using the available tools is able to produce a stable focal mechanism within error bounds.

The alternative hypothesis is supported if the range of uncertainty in the moment tensor due to velocity structure errors is small enough that reasonable conclusions can be made.

Quantitatively, this means that the maximum angle $\theta < 0.21$ and the fault strike uncertainty is no more than 20 degrees. In the case that Alternative Hypothesis 1 is accepted, the following hypotheses are also adopted:

NULL HYPOTHESIS 2:

The focal mechanism for the 6/25/2021 earthquake studied shows reverse fault motion on a fault aligned with the NE-SW trend of the Fall Line in Maryland (average azimuth = 52°).

The alternative hypothesis is likely true if the fault system is complex or not aligned similarly to fault systems in northern and central Virginia. Earthquakes on small faults might trigger each other through stress transfer or might be triggered by nearby human activity such as quarry blasting or reservoir building. A local stress field may also exist, which results in strike slip or normal faulting mechanisms rather than reverse faulting as suggested by the regional compressive field seen in **Figure 5**.

ALTERNATIVE HYPOTHESIS 2:

The focal mechanism for the studied earthquake shows motion along a reverse fault aligned within 20° of the trend of the Fall Line.

Reverse faulting is indicated by a positive rake/slip value, whereas a negative value indicates normal faulting, and a value close to zero indicates strike slip faulting. The alternative hypothesis is likely to be true if the trend of moderately large fault systems in central and northern Virginia continues into Maryland and into Baltimore specifically, and if the local stress field matches the regional field in eastern North America. An example focal mechanism that supports Alternative Hypothesis 2 is shown in **Figure 11** below.

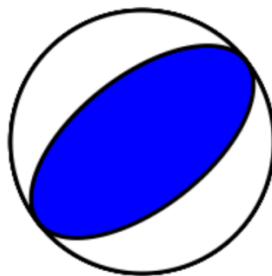


Figure 11: Example reverse faulting moment tensor aligned with the Fall Line

METHOD OF ANALYSIS

MATHEMATICAL BACKGROUND

Moment tensor inversion is a method of reconstructing the focal mechanism, or source motion, at the presumed fault. The moment tensor is a matrix representation of forces (and hence motions) at the source. The inversion procedure relies on the fact that the Earth acts as a filter on the source motions. In other words, the layers of rock through which seismic waves travel modify the original source motions so that they create the signal seen in a seismogram. This filtering effect can be represented in a Green's matrix. Each column of this matrix corresponds to the effects of a simple one-component moment tensor. These fundamental moment tensors can be added and scaled to form any possible moment tensor, just as the x, y, and z unit vectors can be added and scaled to form a vector in 3D space. These 6 simple moment tensors are shown below:

$$M_{11} = \begin{bmatrix} 1 & 0 & 0 \\ 0 & 0 & 0 \\ 0 & 0 & 0 \end{bmatrix}, M_{22} = \begin{bmatrix} 0 & 0 & 0 \\ 0 & 1 & 0 \\ 0 & 0 & 0 \end{bmatrix}, M_{33} = \begin{bmatrix} 0 & 0 & 0 \\ 0 & 0 & 0 \\ 0 & 0 & 1 \end{bmatrix}$$
$$M_{12} = \begin{bmatrix} 0 & 1 & 0 \\ 1 & 0 & 0 \\ 0 & 0 & 0 \end{bmatrix}, M_{13} = \begin{bmatrix} 0 & 0 & 1 \\ 0 & 0 & 0 \\ 1 & 0 & 0 \end{bmatrix}, M_{23} = \begin{bmatrix} 0 & 0 & 0 \\ 0 & 0 & 1 \\ 0 & 1 & 0 \end{bmatrix}$$

Each column of the Green's matrix corresponds to one of the fundamental moment tensors. It is the seismogram data produced when a ground motion represented by that moment tensor is transmitted through a given seismic velocity structure from the source to all the stations. The seismograms for all components (e.g. East, North, Up) of all stations are pasted together to create the columns (see **Equation 1**). Seismic stations employ up to 3 components, which measure movement in different directions.

Multiplying the Green's matrix **G** by the moment tensor **m** is the equivalent of applying a "ground response" filter to the source motion. The result should be the seismograms seen at each station. This is the data vector **d**, which is created by pasting together all the seismograms recorded for each component at each station into a long array. This is the moment tensor equation, represented mathematically as **Equation 1**. Note that in the Green's matrix below, station and component are represented by "s" and "c." N is the number of seismic stations used.

$$\mathbf{d} = \mathbf{G} \mathbf{m}$$

Equation 1

$$\begin{bmatrix} \text{station 1, component 1} \\ \text{station 1, component 2} \\ \text{station 1, component 3} \\ \vdots \\ \text{station N, component 1} \\ \text{station N, component 2} \\ \text{station N, component 3} \end{bmatrix} = \begin{bmatrix} M_{11} s1 c1 & M_{22} s1 c1 & M_{33} s1 c1 & M_{12} s1 c1 & M_{13} s1 c1 & M_{23} s1 c1 \\ M_{11} s1 c2 & M_{22} s1 c2 & M_{33} s1 c2 & M_{12} s1 c2 & M_{13} s1 c2 & M_{23} s1 c2 \\ M_{11} s1 c3 & M_{22} s1 c3 & M_{33} s1 c3 & M_{12} s1 c3 & M_{13} s1 c3 & M_{23} s1 c3 \\ \vdots & \vdots & \vdots & \vdots & \vdots & \vdots \\ M_{11} sN c1 & M_{22} sN c1 & M_{33} sN c1 & M_{12} sN c1 & M_{13} sN c1 & M_{23} sN c1 \\ M_{11} sN c2 & M_{22} sN c2 & M_{33} sN c2 & M_{12} sN c2 & M_{13} sN c2 & M_{23} sN c2 \\ M_{11} sN c3 & M_{22} sN c3 & M_{33} sN c3 & M_{12} sN c3 & M_{13} sN c3 & M_{23} sN c3 \end{bmatrix} \begin{bmatrix} M_{11} \\ M_{22} \\ M_{33} \\ \vdots \\ M_{12} \\ M_{13} \\ M_{23} \end{bmatrix}$$

$$(N \cdot 3 \cdot \text{data length}) \times 1 = (N \cdot 3 \cdot \text{data length}) \times 6 \quad 6 \times 1$$

The columns of the Green's matrix must be computed using a knowledge of the local seismic velocity structure. For large earthquakes recorded at long distances from the source, the seismic waves must travel deep into the Earth, and general Earth models such as PREM can be used. However, for local earthquakes whose seismic waves travel mostly through the crust and uppermost mantle, it is important to have a local velocity structure. This velocity structure can be used to calculate synthetic seismograms for each of the component moment tensors, thus filling out the matrix. Calculating the synthetics is a computationally intensive problem.

In **Equation 1**, \mathbf{m} is a vector made of the components of the moment tensor for the earthquake. Essentially, each component indicates how much each of the fundamental moment tensors M_{11} , M_{22} , M_{33} , M_{12} , M_{13} , M_{23} contribute to the true moment tensor. To solve for the moment tensor of an earthquake, **Equation 1** must be inverted to form **Equation 2**:

$$\mathbf{m} = \mathbf{G}^{-1} \mathbf{d} \quad \text{Equation 2}$$

Luckily, it is not necessary to calculate \mathbf{G}^{-1} . In fact, by strict linear algebra rules, it does not exist, since \mathbf{G} is not a square matrix. In practice, \mathbf{m} can be computed by performing a least squares inversion with \mathbf{G} and \mathbf{d} . This operation finds the \mathbf{m} that minimizes the sum of squared residuals of \mathbf{Gm} and \mathbf{d} i.e. minimizes the sum of squared differences of the elements of \mathbf{Gm} and \mathbf{d} . Least squares inversion is a trivial operation for a computer.

Inverting for the moment tensor involves two separate problems:

- 1) a "forward" problem of finding an appropriate velocity model to fill out the Green's matrix with synthetic seismograms, and
- 2) an "inverse" problem of calculating the moment tensor from Green's matrix and the data vector.

THE FORWARD PROBLEM

Given the importance of determining an accurate velocity structure, two approaches were taken with an eye to quantifying and reducing error in the model. A 1-dimensional flat layered velocity structure is used to simplify calculation as well as to satisfy the requirements of the synthetic seismogram generating program. First, previously existing local seismic velocity models were examined. These models were taken from a variety of sources and were designed for locations from central Virginia to southeastern Pennsylvania.

In order to further constrain the model, surface wave dispersion (SWD) curves developed by Ekstrom (2017) for a location near Germantown, MD, (latitude 39.21, longitude -76.95) were used to construct a shear velocity profile. Surface waves (Love and Rayleigh waves) decay with

depth after about 1 wavelength and thus sample different depths at different wavelengths. Surface waves are also dispersive, meaning that wave velocity is not simply the product of frequency and wavelength (often expressed as $c = f\lambda$). Instead, there is a more complicated relation, or dispersion relation, $c = c(f)$, which when plotted forms a curve known as a dispersion curve. The x-axis typically plots frequency or period, while the y-axis plots shear-wave velocity (V_s). This relation is dependent on the shear-velocity structure of the Earth and so can be inverted to produce a shear velocity model. An empirical relationship between V_p and V_s developed by Brocher (2005) is used to estimate a P-wave velocity profile from the results for comparison with local models.

A Python code developed by Fabrizio Magrini (Magrini, 2023) performs a transdimensional Bayesian inversion on the dispersion curves. This produces a statistical ensemble of models with a varying number of layers based on the SWD data and an initial model guess input into the program. The permitted standard deviation of the results can be adjusted to allow for more flexibility in fitting the data. The maximum number of layers in the resulting models can also be changed. The range of reasonable models is inferred from the density of the spread of models. A high density of models with a certain shear velocity at a given depth means that a model with this velocity at this depth fits the data well. Both Rayleigh and Love wave data were used in the inversion, which helped to better constrain the model results.

THE INVERSE PROBLEM

Producing synthetic seismograms:

Once a velocity model is chosen, it is used to produce synthetic seismograms for all the components (e.g. East, North, Vertical) of all the receiving stations. These are calculated using Pyprop8, an open-source Python program developed by Andrew Valentine (Valentine, 2022) based on an algorithm by O'Toole and Woodhouse (2011). Pyprop8 is a lightweight package that uses a 1-dimensional velocity model with four parameters: P-velocity (V_p) in km/s, S-velocity (V_s) in km/s, density (ρ) in g/cm³, and layer thickness in km. It also assumes the flat Earth approximation, and thus is only valid for up distances up to 200 km. The algorithm was used by O'Toole et al. (2012) to calculate moment tensors for 2005 Fukuoka earthquake using GPS displacement data filtered between 0.05 and 0.2 Hz. For velocity models that do not specify V_s or ρ or a relationship between them the following empirical relationships from Brocher (2005) were used:

$$V_s = 0.7858 - 1.2344V_p + 0.7949V_p^2 - 0.1238V_p^3 + 0.0064V_p^4 \quad \text{Equation 3}$$

$$\rho = 1.6612V_p - 0.4721V_p^2 + 0.0671V_p^3 - 0.0043V_p^4 + 0.000106V_p^5$$

Station selection and data processing:

The coordinates for the epicenter of the 6/25/21 Baltimore earthquake and all stations within 200 km were found on the ISC, Earthscope Wilber3, and Raspberry Shake databases. Velocity waveform data (units: m/s) for all stations and all components were bandpass filtered

and plotted using the EarthScope Sage URL builder. Many stations did not have any data, and some had data that was too noisy to use. Stations were accepted if the SNR for the highest peaks was above 4 when filtered below 1 Hz. The upper limit of 1 Hz was chosen to make waveforms easier to fit (the higher the frequency, the harder it is to fit a significant section of the waveform). 0.5 Hz was also chosen as a lower limit, since below this frequency the waveform noise rises rapidly. In total, five stations were used from the Wilber3 database. In addition, two stations with acceptable data were found on the Raspberry Pi seismic network. Station locations are plotted in **Figure 12**.

For each of the five Wilber3 stations, two minutes of waveform data for each earthquake starting at the event time was then downloaded as a miniseed file and imported into Python. An extra 45 seconds of data before the event was imported for the two Raspberry Shake stations to eliminate mathematical artifacts produced by filtering. The mean was removed from all data to ensure that waveforms were centered at zero. The 0.5 – 1.0 Hz frequency range was used for the corner frequencies of a 4th order Butterworth bandpass filter that was applied to the data. The data were then resampled from 100 Hz to 10 Hz using an interpolation function to save computation time. This step also allowed the lengthened time series to be clipped to remove mathematical artifacts. All stations had three components measured with the same (East, North, Vertical) coordinate system as Pyprop8, except RAD82, which only has a vertical component.

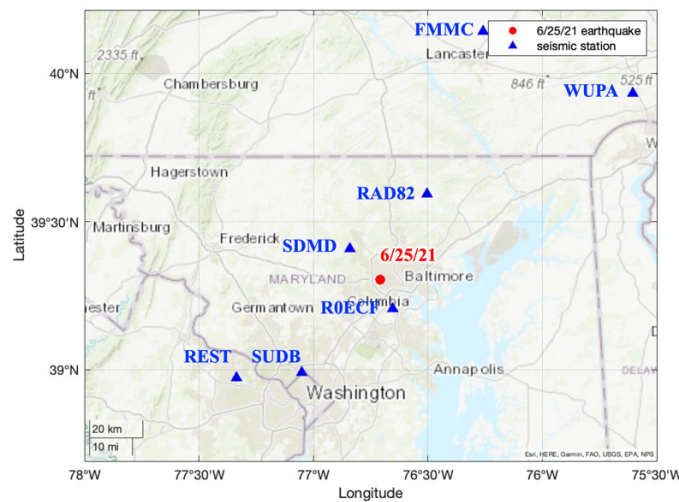


Figure 12: Stations used in the inversion

Next, the 6 fundamental moment tensors were created in Python. Each of these was input into Pyprop8 to create synthetic displacement seismograms (units: mm) at all the stations. The synthetic data were then differentiated to produce velocity seismograms, which were pasted together into the columns of the Green's matrix **G**. The data vector was multiplied by 1000 to accord with the units used by Pyprop8 and then pasted together to create the data vector **d**. Finally, only the highest amplitude S and surface waves were counted for the inversion. All parts of the data and synthetic waveforms outside this time window were set to zero so that they would not affect the inversion. Time windows selected for each station are recorded in **Table 2**.

Bandpass corner frequencies: 0.5 Hz – 1 Hz

| Station | Latitude | Longitude | Azimuth | Window Start (s) | Window End (s) | Channels | Database |
|---------|-----------|------------|---------|------------------|----------------|----------|----------|
| SDMD | 39.41017 | -76.84033 | 316° | 3 | 11 | 3 (ENU) | Wilber3 |
| SUDB | 38.99 | -77.05 | 220° | 12 | 20 | 3 (ENU) | Wilber3 |
| FMMC | 40.14 | -76.26 | 22.3° | 28 | 35 | 3 (ENU) | Wilber3 |
| WUPA | 39.9324 | -75.606 | 53.2° | 34 | 42 | 3 (ENU) | Wilber3 |
| REST | 38.972527 | -77.377348 | 237° | 18 | 24 | 3 (ENU) | Wilber3 |
| R0ECF | 39.207207 | -76.654731 | 122° | 1 | 7 | 3 (ENU) | R Shake |
| RAD82 | 39.594594 | -76.503509 | 28.6° | 11 | 16 | 1 (U) | R Shake |

Table 2: Stations used for inversion. Azimuth is the angle from North between source and station. Columns 5 to 6 show the time windows used for each station in the inversion. The Channels column shows the number and orientation of component seismograms (ENU = East, North, Up). RAD82 only has an Up vertical component. The source of the data is given in the last column (R Shake = Raspberry Shake).

The inversion is performed using a least squares inverse, as explained in the Mathematical Background section. The resulting moment tensor is decomposed into a deviatoric and best double couple component and displayed as a beachball diagram using the Pyrocko seismology Python package (Heimann et al., 2017). Note that the moment tensor must be rotated from the ENU (East, North, Up) coordinate system used by Pyprop8 to the NED (North, East, Down) system understood by Pyrocko.

Finally, earthquake depths given on the Wilber3 database are often unreliable, as shown by many seismic events that probably originate from near surface explosions and which were eliminated in **Figure 1B** but are assigned depths of up to 13 km in Wilber3. The depth of the 6/25/21 earthquake was determined by performing an inversion at depth intervals of 1 km down to 19 km. For each depth, the variance reduction (**Equation 4**), a measure of the misfit between the data and the inversion, was calculated. The depth that maximized variance reduction was chosen as the true depth.

$$\text{Variance Reduction} = 1 - \frac{\text{variance}(\text{inversion}) - \text{variance}(\text{data})}{\text{variance}(\text{data})} \quad \text{Equation 4}$$

All code for the inversion was written by the author of this research with assistance from Dr. Vedran Lekic. The inversion code is included Appendix B.

ANALYSIS OF UNCERTAINTY

The majority of the uncertainty is assumed to come from an inaccurate knowledge of the velocity structure and other properties of the Earth and from the failure to incorporate these many heterogeneous factors into calculating the synthetics. This includes error from the 1-dimensional, flat layer assumption as well as from possibly not using the best 1-D model. Error also comes from noise in the signal, which is especially troublesome at farther stations. However, given the difficulties of determining model uncertainty, assigning a number to it, and then propagating it with signal uncertainty, an empirical approach is adopted.

The model uncertainty can be mapped onto a maximum uncertainty in the focal mechanism in the following way. A selection of reasonable models (in this case, 4 models) is chosen based on the results of the forward problem. These can be thought of as the “model space.” Each of these models is used to compute a moment tensor. If each moment tensor is represented as a 6-dimensional vector (recall the moment tensor has 6 independent components), the angle in six-dimensional space between two moment tensors **A** and **B** can be computed by the following formula:

$$\theta = \cos^{-1} \frac{\mathbf{A} \cdot \mathbf{B}}{\|\mathbf{A}\| \|\mathbf{B}\|} \quad \text{Equation 5}$$

Where $\mathbf{A} \cdot \mathbf{B}$ represents the dot product of **A** and **B**, and $\|\mathbf{A}\|$ represents the norm (or length) of **A**

This angle is normalized to 1 (maximum error = 1) for easy comparison.

This angle serves as a measure of the difference between moment tensors. Note that it does not take earthquake magnitude into account. To return to the problem at hand, Equation 3 can be used to compare the set of computed moment tensors with each other. If this maximum angle falls above a certain threshold for similarity (Chosen as $\theta = 0.21$ for reasons explained below) then the Null Hypothesis 1 is indicated. In other words, no meaningful conclusions can be made from the moment tensor solution because error from the velocity model produces too much error in the solution. On the other hand, if the maximum angle falls below $\theta = 0.21$, then the moment tensor solution is stable and Alternative Hypothesis 1 is indicated. Because this method relies on computing moment tensors with real data, it has the added benefit of including error from signal noise as well.

The threshold error of $\theta = 0.21$ was chosen based on statistical analysis of error for random moment tensors. A test moment tensor was chosen by assigning uniformly distributed pseudorandom numbers between -10000 and 10000 to each of the six components. One million more moment tensors were then computed in the same way, and for each the angle between it and the test moment tensor was computed. These 1 million angles were then plotted on a histogram (**Figure 13**) with 1000 bins. The bin number (and corresponding angle) above which 98% of the counts fell was then determined. Running this analysis several times and averaging yielded a threshold angle of $\theta = 0.21$. Note that the threshold for 99% chance of similarity is $\theta = 0.18$.

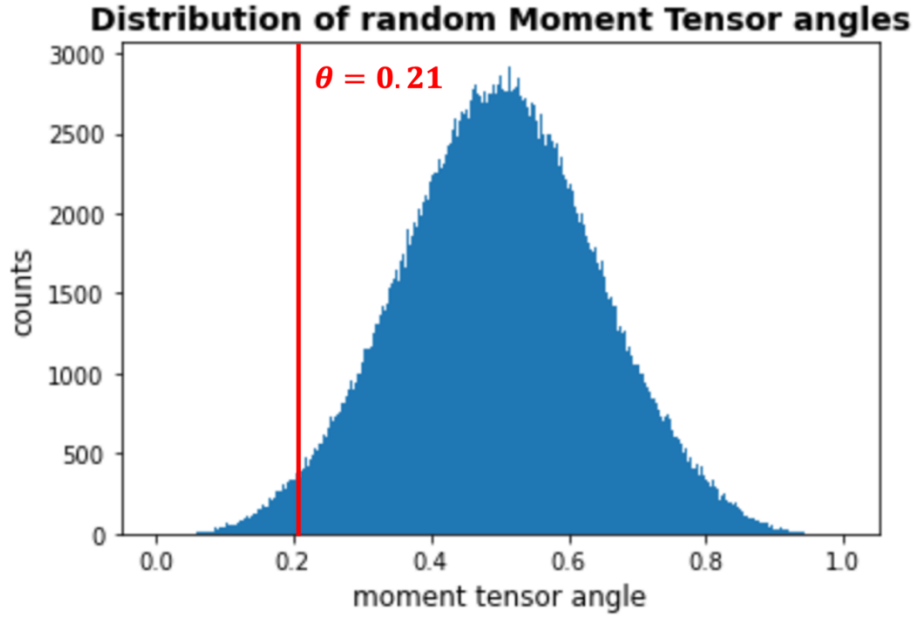


Figure 13: histogram of random moment tensor angles. 98% of angles fall above the 0.21 threshold. In other words, if a moment tensor angle falls below $\theta = 0.21$, there is a 98% probability that the similarity is not due to random chance.

Because the goal of this research is to find a fault plane solution, the model uncertainty is also mapped onto uncertainty in strike, dip, and rake. This is given by the maximum difference in these values between fault plane solutions produced by the best double couple solutions of the moment tensor. A difference of 20° in strike, dip, and rake is set as the threshold for fault motion similarity. If the difference between the strike, dip, or rake produced by one model in the model space is more than 20° off from its corresponding value produced by another model, then Null Hypothesis 1 is supported. If all of these values fall below 20° , then Alternative Hypothesis 1 is supported i.e. meaningful conclusions about the fault plane solution can be made. The approach for error analysis is depicted graphically in **Figure 14**.

In this case, the same 20° threshold can be used to test Null Hypothesis 2. Namely, if the strike of both fault plane solutions is greater than 20° away from the Fall Line (average azimuth = 52°), then the trend of the fault is not considered to be aligned with the Fall Line. However, if either of the fault plane solutions is within 20° of the Fall Line, then the fault is considered aligned, and Alternative Hypothesis 2 is supported.

Note that for proper error analysis more than four models in the model space should be used to find the maximum 6-dimensional angle and the maximum strike, dip, and rake differences. Ideally, a Monte Carlo simulation using several hundred to several thousand models should be implemented. However, the computational intensity required to test so many models is beyond the scope of this research.

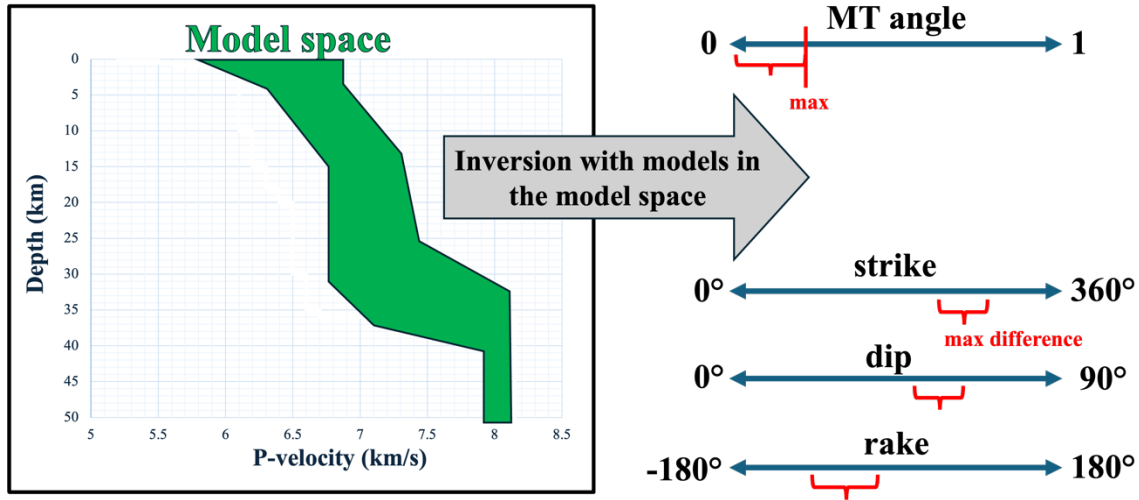


Figure 14: Graphical explanation of uncertainty analysis.

PRESENTATION OF DATA

THE FORWARD PROBLEM

The goal of this part is to constrain a “model space,” or range of likely velocity models that is limited enough that all models within this range will produce similar inversion results.

Local models for P-wave velocity structures are plotted in **Figure 15A**. Although almost all earthquakes occur in the Piedmont, two models from the Coastal Plain were included, since they should be similar to the other models below a few km in depth. Some models do not extend all the way to the Moho. All models except the SE Pennsylvania model and Charlottesville E1 model were compiled by Mooney and Boyd (2021) in a database of 1-D velocity structures for the Central and Eastern United States. Data for all velocity structures is given in Appendix A. The highlighted models are used in the inversion.

| Model Name (Location) | Province | Max Depth | Original Source |
|---------------------------|-----------------|--------------|--------------------------------------|
| Charlottesville W | Piedmont | 39 km | Bollinger et al. (1980) |
| Millville (NJ) - Coast | Coastal Plain | 8.5 km | Sheridan et al. (1991) |
| Richmond W | Piedmont | 0.7 km | Bollinger et al. (1980) |
| Charlottesville E1 | Piedmont | 36 km | Chapman (2013) |
| Ocean City (NJ) | Coastal Plain | 32.6 km | Gaherty et al. (2009) |
| Silver Spring | Piedmont | 34 km | James et al. (1968) |
| Charlottesville E2 | Piedmont | 2 km | Bollinger et al. (1980) |
| Richmond E | Piedmont | 36 km | Munsey & Bollinger (1985) |
| SE Pennsylvania | Piedmont | 37 km | Nyblade & Homman (2016) |

Table 3: Local models used to constrain the velocity model. Model names give the location for which the model was made e.g. Charlottesville W means a few km West of Charlottesville. The maximum depth for which the models provide data is also given.

The models have significant spread below 18 km depth. This distribution is bimodal with 4 models showing a velocity around 6.1 km/s and two showing a much higher velocity of about 6.5 km/s. Between 20 and 30 km depth, the models are tightly constrained, varying only between a 6.4 and 6.6 km/s. The upper mantle velocity is even more tightly constrained at around 8.1 km/s. The models are less clear about the Moho depth, which varies between 34 and 39 km. This is unsurprising in light of the findings of Soto-Cordero et al. (2018) referenced in the background section, which show a steep trend in Moho depth over the Piedmont. The best general model might use an average Moho depth value. The models also disagree on a possible transition (gradual or sudden) from about 6.1 km/s to about 6.5 km/s above 20 km depth.

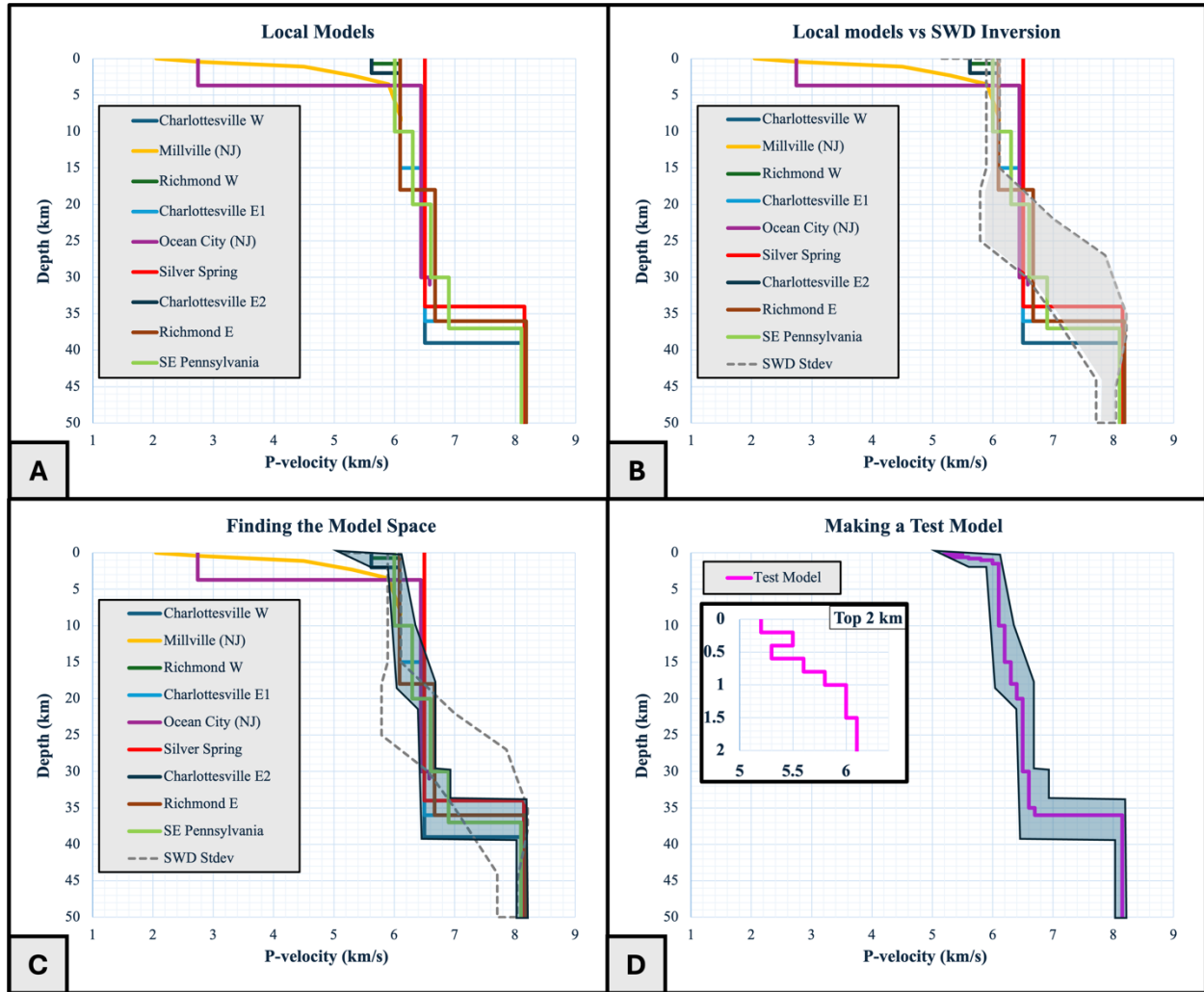


Figure 15: Steps of the forward problem A) Local velocity models. B) SWD inversion compared with local models. C) Constraining the model space by finding where models overlap most. D) creating a test model within the model space. This model is used to test the results of a random model within the model space. Inset shows detail of the top 2 km, including a low velocity zone.

Information for the SWD model is shown in **Figure 16**. The top left panel (A) shows the initial model guess as well as the range of models the program is permitted to explore. The top right panel (B) shows the Love and Rayleigh dispersion data found by Ekstrom (2017), which ranges in period from 5 s to 40 s. Also shown are the dispersion curves produced by the initial model guess (misleadingly called the “True” model). The statistical range of dispersion curves produced by the inversion is shown as colored bands that attempt to fit the data. The permitted standard deviation of dispersion curves for both Love and Rayleigh was set to 0.02, while the number of layers allowed was set to between 3 and 4. Setting a high number of layers can yield unrealistic low velocity layers in the results, since the program tries to fit the data without regard for geology. The bottom panel (C) shows two chains, or implementations, of the inversion with very similar results.

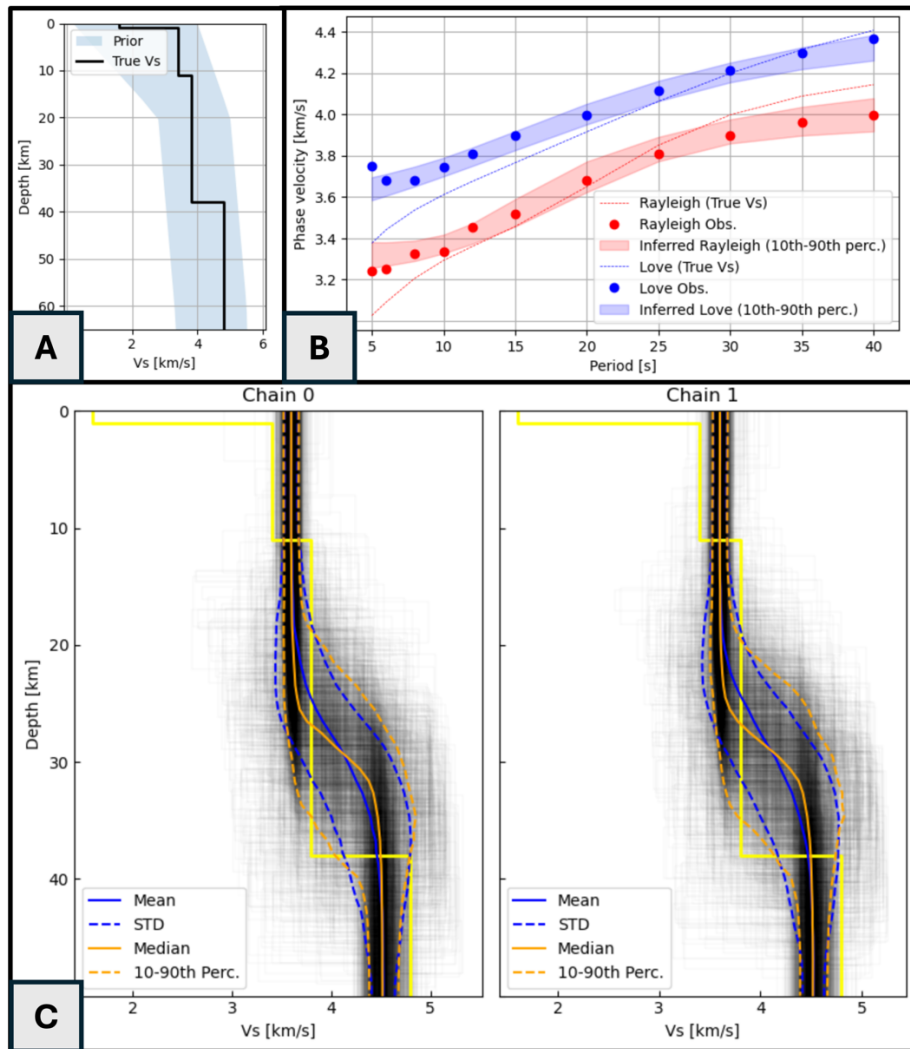


Figure 16: Surface Wave dispersion data. A) The initial model guess and allowed range of models. B) Surface wave dispersion data for Rayleigh and Love waves: both were used in the inversion. Data was collected at coordinates (39.21, -76.95) in Maryland. Also shown are the initial guess (‘true’) model dispersion curves and the range of curves produced by the inversion. C) Statistical data for the inversion. The yellow line is the starting model. Darker areas indicate higher certainty.

V_p relationships were recovered from the V_s data using **Equation 3**. The range of SWD models within one standard deviation is shown in **Figure 15B**, where it is compared with the local velocity models. Above 15 km, V_p is tightly bound between 6 and 6.2 km/s. This strongly supports the local models that show a seismic velocity of about 6.1 km/s in the first 10 km of crust. Based on the similarity of the SWD model and four other models in this range (Millville, Charlottesville E1, Richmond E, & SE Pennsylvania), the data from the Silver Spring and Ocean City models showing much higher velocity in this depth range are excluded from the model space. The sudden increase in uncertainty in the SWD model at 15 km may suggest a velocity transition here. Below this point the SWD data is not well constrained until about 45 km, where it becomes tightly bound between 7.8 and 8.1 km/s. This does not help constrain the model further, however, since the local velocity models agree on the upper mantle velocity within 0.1 km/s.

Note that because the lowest period used by the inversion is 5 s, the inversion is likely to miss layers in the first kilometer or two. Other geophysical models also may miss near-surface details. Therefore, a region of low velocity near the surface was included in the model space, in agreement with the Richmond W and Charlottesville E2 models. The model space created by comparing the local models and the SWD inversion is shown as a blue shaded region in **Figure 15C**. Finally, a test model (**Figure 15D**) constrained by the model space was created. This was given more gradual increases in velocity as well as a low velocity zone near the surface to represent the effects of a highly variable upper crust.

The models developed by Chapman (2013), Nyblade and Harman (2016), Munsey and Bollinger (1985), as well as the Test Model all fit within the model space and were used in the moment tensor inversion in order to analyze the stability of the moment tensor solution with changes in the velocity model.

THE INVERSE PROBLEM

Earthquake Depth:

Figure 17 shows a plot of variance reduction vs. depth for the four models entirely within the model space. A fifth model by James et al. (1968) for Silver Spring is also included to show the result of using a model outside the model space. The first four models all show prominent maxima between 8 and 9 km, though the Test model and Munsey and Bollinger (1985) show roughly equal maxima at 1 km and 13 km respectively. 9 km was chosen as the depth, since it shows the highest variance reduction on average. The James et al. (1968) model, which partly fell outside the model space, does not show the same trend as the other models. The average variance reduction over all depths is recorded in the table to the right. The first four models show about the same average variance reduction, but the James et al. (1968) model has a much lower value and has lower peaks, indicating that it is less able to fit the data at any depth. This further justifies excluding it from the model space.

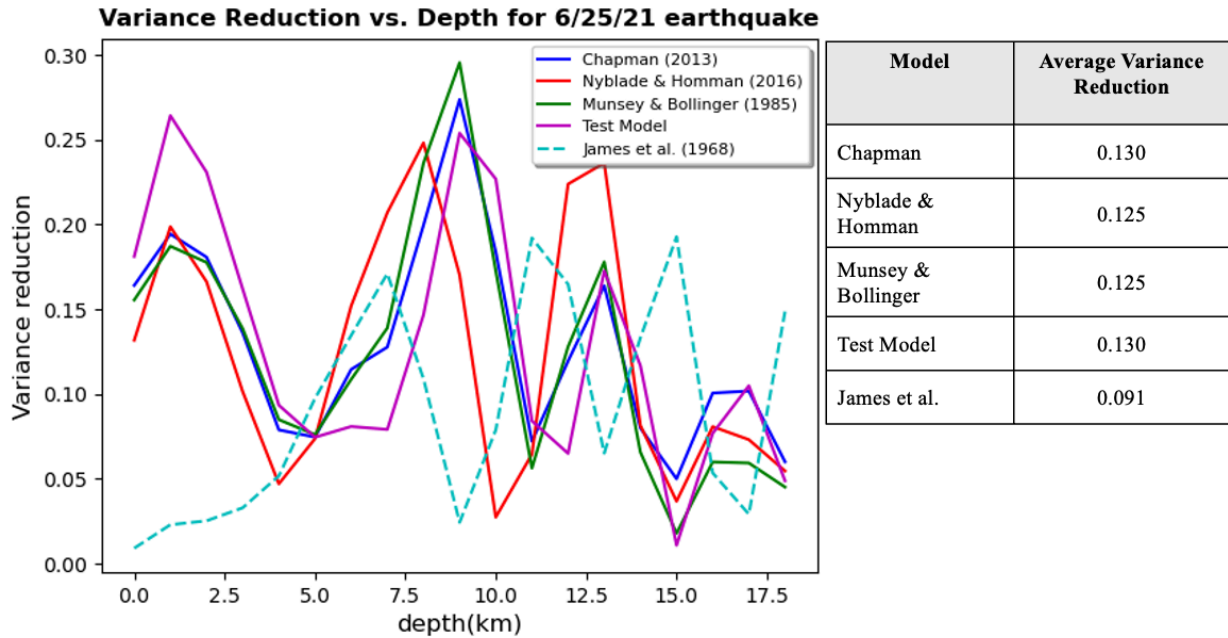


Figure 17: Variance reduction vs. Depth for 5 different models. The four models within the determined model space all show high agreement with the data at 8-9 km. The James et al. model, which was excluded from the model space, has a significantly lower maximum variance reduction, justifying its exclusion.

Inversion Results

Once the inversion was complete, the data waveforms were time-shifted to account for the effects of heterogeneities in the velocity structure. The time shifts were adjusted until variance reduction was maximized. Care was taken to ensure that the initial arrival of high amplitude waves coincided in the data and inversion waveforms. Comparisons between data and inversion waveforms for the four models used are shown in **Figure 18 to 19**. Time shifts for each component are shown on the graph, while the variance reduction is shown at the bottom of each figure.

Moment tensors, focal mechanisms, and fault plane solutions for all four models are depicted in **Figure 22**. The deviatoric and best double couple solutions are shown. The maximum 6-dimensional angle between moment tensors is $\theta=0.043$, far below the threshold for moment tensor similarity, indicating that the moment tensors have a 99.995% chance of being related. The maximum strike, dip and rake differences are 12° , 5° , and 15° respectively, within the set limit of 20° for similarity of fault plane solutions. Note that the greatest difference comes from the Test Model, indicating that the velocity model might need to be narrowed farther to get a more exact solution.

The moment tensor decomposition has been plotted on a Hudson diagram in **Figure 23A**. **Figure 23B** shows the full moment tensor solution for Chapman (2013), including the isotropic component as well as the pressure and tension axes on a stereographic Lambert plot. The other solutions are very similar.

Chapman (2013)

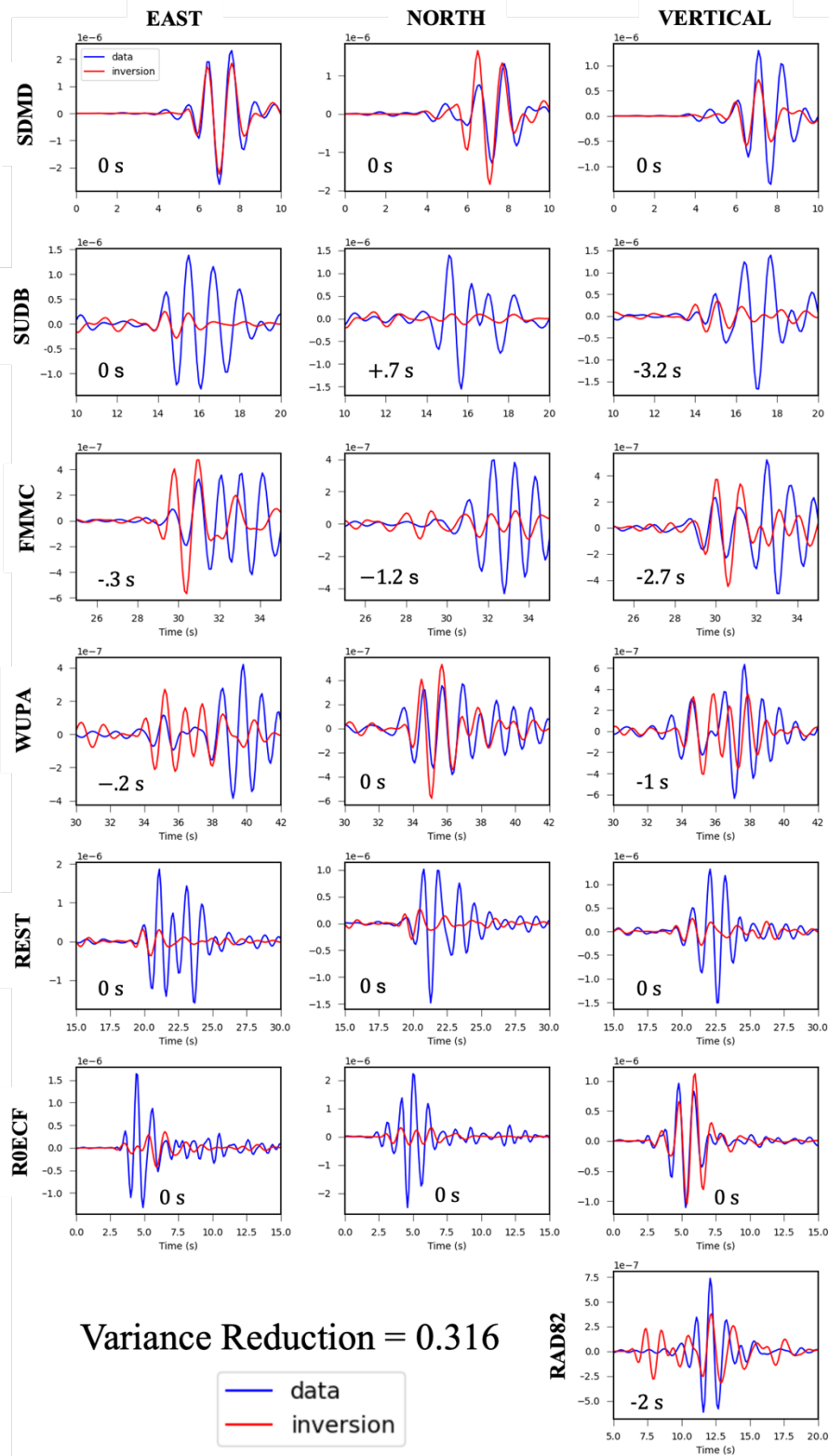


Figure 18: Data vs inversion waveforms for the Chapman (2013) model

Nyblade & Homman (2016)

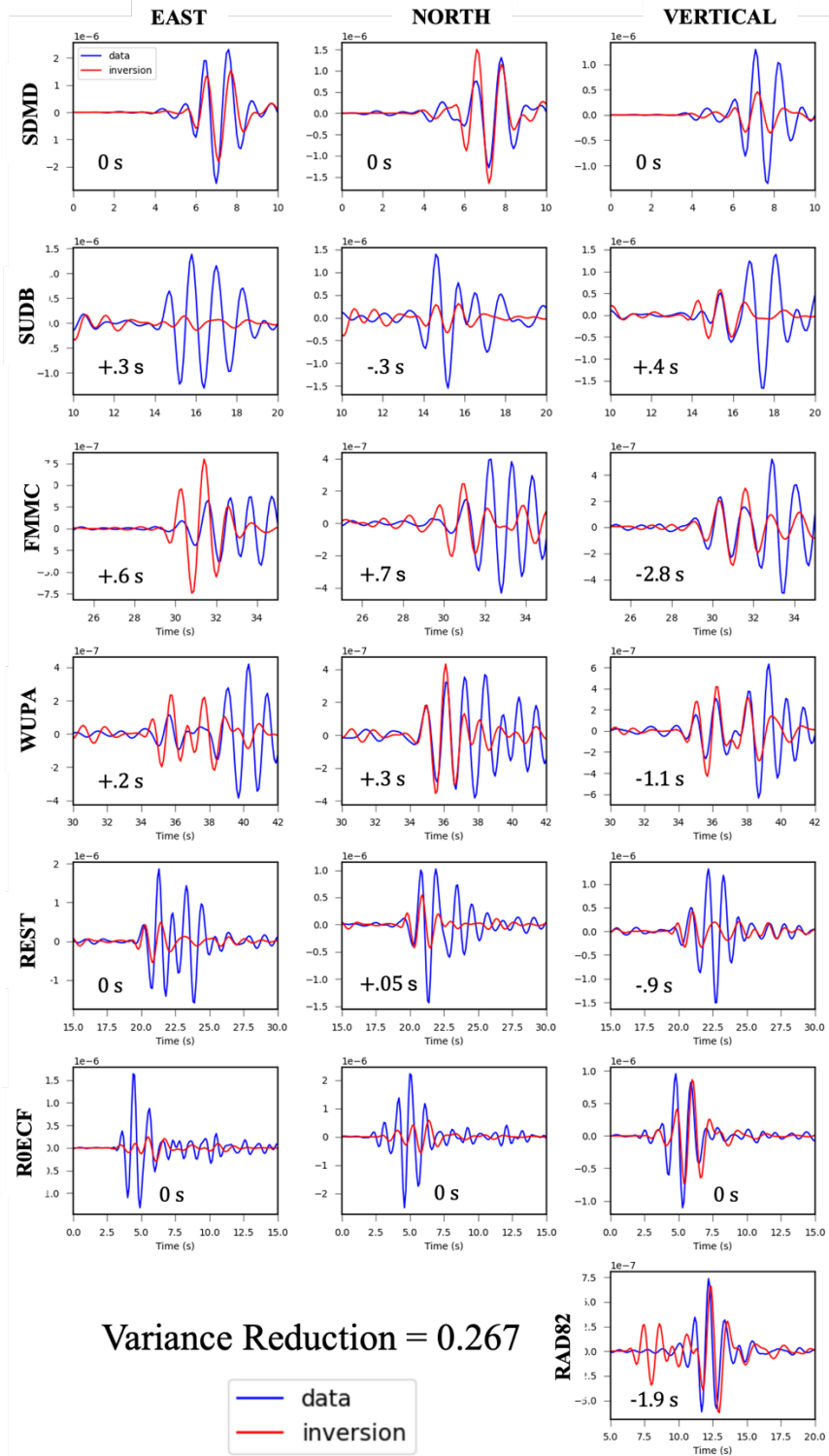


Figure 19: Data vs inversion waveforms for the Nyblade & Homman (2016) model

Munsey & Bollinger (1985)

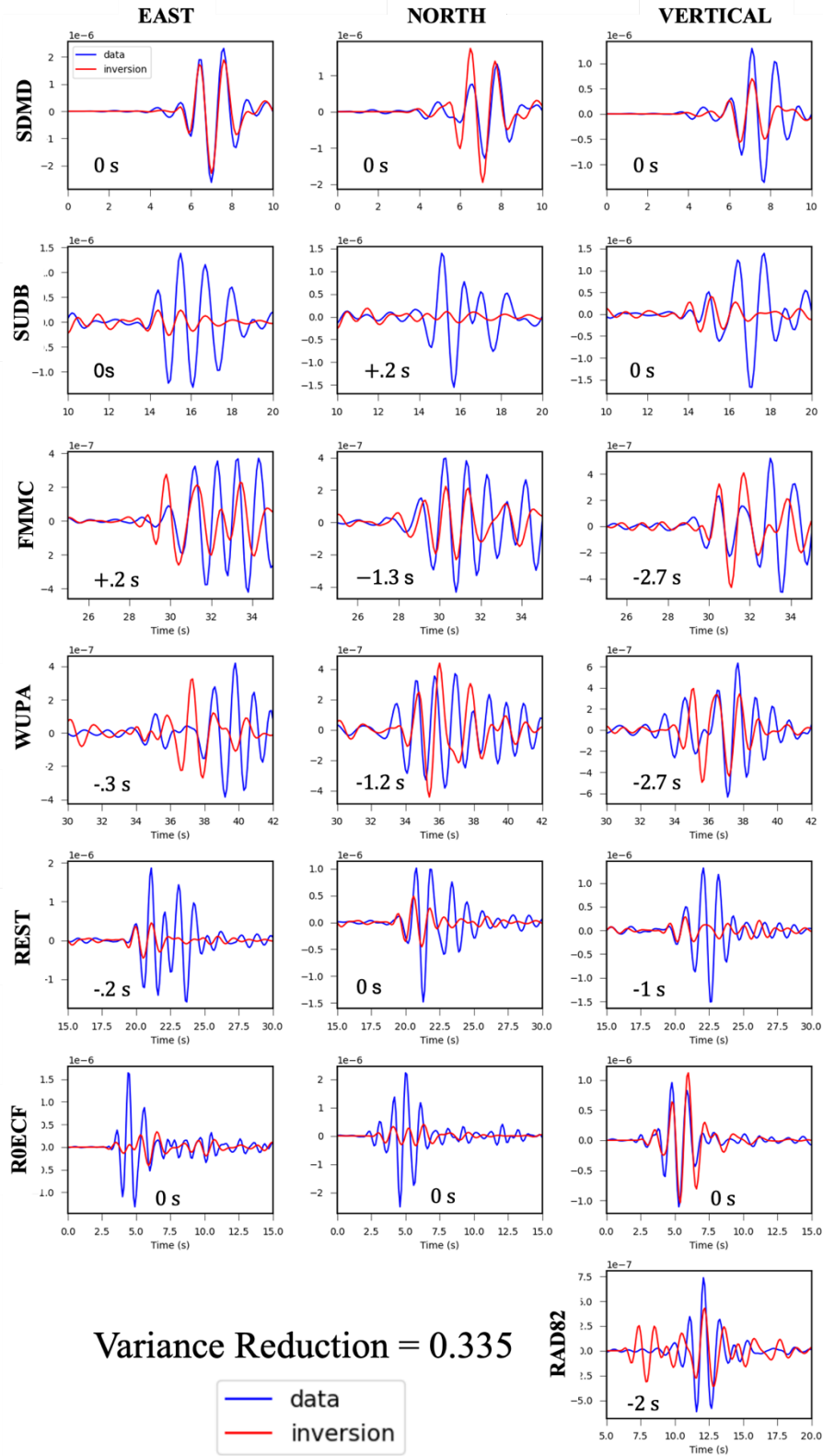


Figure 20: Data vs inversion waveforms for the Munsey & Bollinger (1985) model

Test Model

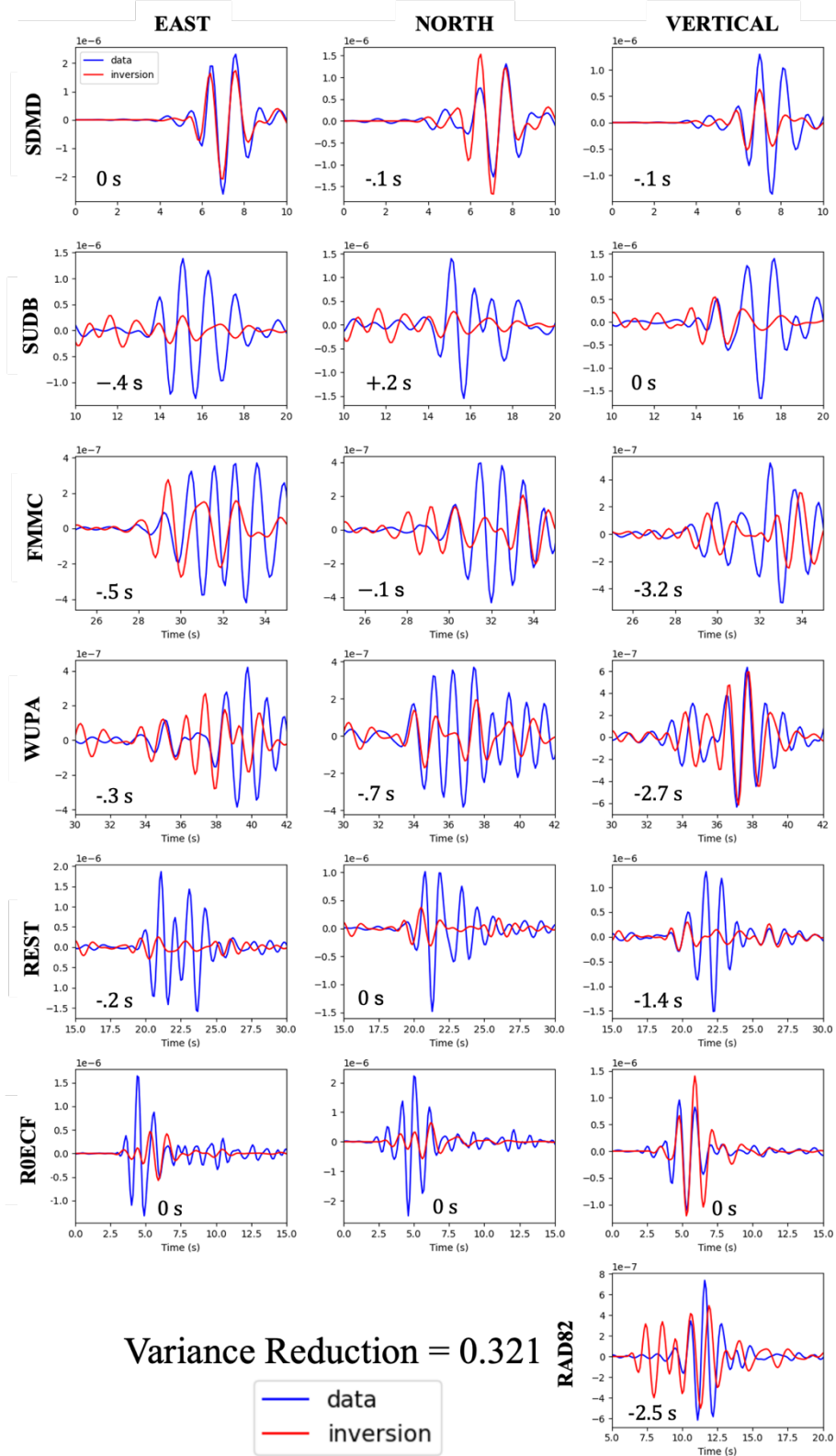
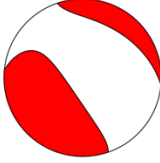
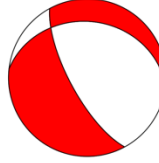
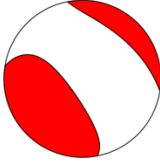
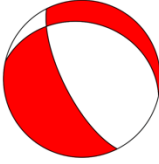
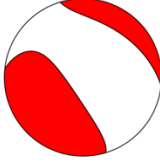
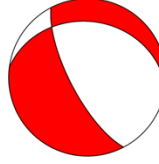
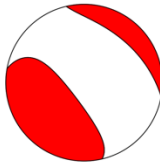
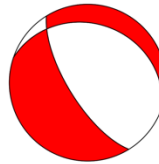


Figure 21: Data vs inversion waveforms for the Test Model

| Model | Moment Tensor ($\times 10^{12} N \cdot m$) | Deviatoric | Best Double Couple | Fault Plane Solution | | |
|---------------------------------|---|---|--|-----------------------------------|---------|---------|
| Chapman (2013) | $\begin{bmatrix} 11.3 & 9.9 & 11.5 \\ 9.9 & 16.1 & 6.0 \\ 11.5 & 6.0 & 1.1 \end{bmatrix}$ $M_w = 2.77$ |  |  | | Plane 1 | Plane 2 |
| | | | | Strike | 276 | 152 |
| | | | | Dip | 29 | 72 |
| | | | | Rake | -142 | -66 |
| | | | | P-axis = 92° T-axis = -137° | | |
| Nyblade & Homman (2016) | $\begin{bmatrix} 13.3 & 11.7 & 10.7 \\ 11.7 & 14.1 & 6.6 \\ 10.7 & 6.6 & 1.6 \end{bmatrix}$ $M_w = 2.78$ |  |  | | Plane 1 | Plane 2 |
| | | | | Strike | 282 | 152 |
| | | | | Dip | 29 | 71 |
| | | | | Rake | -137 | -68 |
| | | | | P-axis = -13° T-axis = -137° | | |
| Munsey & Bollinger (1985) | $\begin{bmatrix} 12.7 & 11.2 & 12.2 \\ 11.2 & 17.0 & 6.5 \\ 12.2 & 6.5 & 1.6 \end{bmatrix}$ $M_w = 2.80$ |  |  | | Plane 1 | Plane 2 |
| | | | | Strike | 277 | 152 |
| | | | | Dip | 30 | 72 |
| | | | | Rake | -142 | -66 |
| | | | | P-axis = 94° T-axis = -133° | | |
| Test Model | $\begin{bmatrix} 16.3 & 13.8 & 13.6 \\ 13.8 & 17.8 & 9.1 \\ 13.6 & 9.1 & 0.5 \end{bmatrix}$ $M_w = 2.84$ |  |  | | Plane 1 | Plane 2 |
| | | | | Strike | 288 | 148 |
| | | | | Dip | 25 | 70 |
| | | | | Rake | -127 | -74 |
| | | | | P-axis = 83° T-axis = -134° | | |
| | | | | Average Solution | | |
| | | | | | Plane 1 | Plane 2 |
| | | | | Strike | 281 | 148 |
| | | | | Dip | 28 | 70 |
| | | | | Rake | -137 | -74 |
| | | | | P-axis = 64° T-axis = -135° | | |

$\theta_{\max} = 0.043$

max strike difference = 12°

max dip difference = 5°

max rake difference = 15°

$$\theta_{\max} = 0.043$$

max strike difference = 12°

max dip difference = 5°

max rake difference = 15°

Figure 22: Inversion results for the four models. Moment tensors are given along with the calculated moment magnitude (M_w), deviatoric focal mechanism, and best double couple focal mechanism. Both fault plane solutions are also given along with P-axis and T-axis azimuths. The maximum 6-dimensional angle and maximum differences in strike, dip, and rake are shown at the bottom.

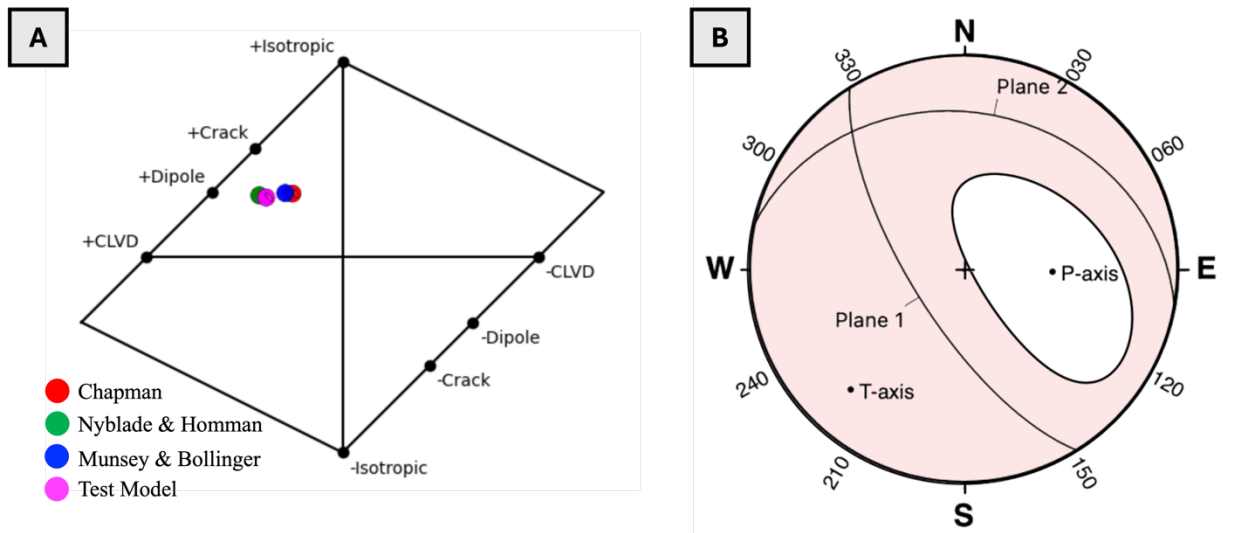


Figure 23: Full moment tensor information. A) Hudson plot of all four solutions. B) Full moment tensor for Chapman (2013) with fault plane solutions and pressure (P) and tension (T) axes shown. Stereonet11 (Allmendinger, 2013) was used to plot planes and axes. Other moment tensors are very similar in appearance, though the P-axis is significantly different for the Nyblade and Homman (2016) model.

DISCUSSION OF RESULTS

The results indicate that moment tensor inversion can produce a stable focal mechanism for at least some small earthquakes in Maryland. The best double couple solution produced for the 6/25/21 Baltimore earthquake shows a primarily normal faulting mechanism, which supports Null Hypothesis 2. This is unexpected, given that the regional stress field for Maryland is compressive.

Fault plane 2 (strike = 148, dip = 70) was chosen as the true fault plane, since it aligns with the NW-SE direction of two of the normal faults mapped in Baltimore (**Figure 9**). While it seems unlikely that these particular faults extend to a depth of 9 km, their orientation may be indicative of other more deeply buried faults that are similarly oriented and originated from similar stress conditions. However, the identification of faults as reverse or normal on a map may not be particularly important, since these faults likely date back to the Alleghenian orogeny at the latest and possibly much earlier. So, local extensional stress could be causing slip to occur on an ancient thrust fault (this would make it more likely that Plane 1 is the true fault solution. It is also possible that slip is occurring along one of the lithological contacts within or below the Laurel Belt.

The stress field is indicated by the P (pressure) and T (tension) axes (**Figure 23B**). The Tensile axis, as the stronger component, is more stable, varying only within 4° in azimuth, while the P-axis, the weaker component, is only stable in azimuth for 3 of the solutions. Interestingly, for these 3 solutions, the azimuth of the P-axis is aligned with the E-W compressive stress field found for Maryland by Levandowski et al. (2018) depicted in **Figure 5**. However, there is a very significant vertical component. Strangely, the tension axis, aligns quite well with the NE-SW maximum compressional stress seen in many parts of eastern North America (compare with the

focal mechanism for Tewksbury, NJ in **Figure 8**). This implies that a local stress field exists in the Baltimore area that is dominantly tensile with maximum tension in the NE-SW direction.

However, the inversion results should be treated with caution. The waveform fits in **Figure 18** through **21** are not especially close. The time shifts employed to fit the waveforms are also concerning, since different components of the same station, which should arrive at the same time, had to be time shifted apart by as much as 3 seconds. This may reflect the arrival of different high amplitude pulses from multi-pathed waves. Noise interference may also be an issue, since a low SNR was accepted for some stations in order to achieve better coverage and hence more stability in the results. Using fewer stations may improve the waveform fit but may yield a less stable solution. Difficulty fitting the waveforms is also likely due to missing information in the velocity model. Reflections and refractions from heterogeneities in the upper crust may create much more complex waveforms than are predicted by the synthetics and may cause waves to attenuate more or less than predicted. For example, the amplitude of the data waveforms was significantly stronger than the synthetics for SUDB and REST stations, which have similar source to station azimuths.

Of additional concern are the high isotropic and CLVD components of the moment tensor solutions, which are likely indicative of error in the modeling process. It is possible that the depth was incorrectly located. The variance reduction vs depth plot showed several other peaks (1 km and 13 km), which might represent the real depth. Finally, as mentioned in the error analysis section, a proper Monte Carlo simulation would be needed to fully map the uncertainty in the model space onto uncertainty in the moment tensor and fault plane solution.

Despite these serious reservations, the results represent an important step forward in interpreting small scale seismicity in intraplate regions with sparse station coverage and low SNR. The ability to find a stable moment tensor solution suggests that, even if further work is needed to confirm or adjust the current results, meaningful information about faulting and stress can be extracted from the waveform data. This is especially true given that this research employed many simplifying assumptions, and computational intensity was minimized as much as possible – the longest programs (depth analysis) took about a half hour to run on a personal laptop. Much more accurate results could be achieved using computationally heavier tools, such as Bayesian algorithms, that examine many more combinations of parameters. Bayesian tools also produce uncertainty estimates, which could supersede the relatively primitive method of examining moment tensor angles and spread of strike, dip, and rake values.

SUGGESTIONS FOR FUTURE WORK

As suggested above, this research should be replicated using a technique that is better able to examine many combinations of parameters (velocity model, depth, and time-shifts) and find a stable, best fitting solution. Additionally, there is uncertainty in the epicentral location, which this research did not directly address (though time-shifts may have corrected for this). Location uncertainty is shown by the spread of recorded seismic events within several kilometers of quarries, mines, and military testing sites, indicating that the epicenters of these probable man-made events are misplaced.

Aside from using better computational tools, further geological and geophysical research can provide valuable information, since one of the principal difficulties in seismic inversion is lack of data. Data sparsity means that more parameters must be investigated, and, of course, results in greater uncertainty. This problem can be addressed in a number of ways. A network of

seismic arrays could be placed in a rough grid across Virginia, Maryland, Pennsylvania, and New Jersey. This network would not just provide more data for studying local seismicity, but also higher signal quality, since more stations would be closer to seismic events. It would also enable the construction of a 3-dimensional velocity model given a sufficiently widespread grid. Such projects have been conducted by state governments before, as was done in Pennsylvania between 2013 and 2015 (Nyblade and Homman, 2016). However, the network need not be fully funded by government or research institutions. Raspberry Shake seismic sensors can be deployed by residents and citizen scientists. Two Raspberry Shake stations were used in this research and helped to make the results possible. What is primarily needed is an outreach program to convince communities organizations such as schools, libraries, and neighborhood associations, as well as ordinary residents to install these sensors. This has been done to some degree at schools; however, many of these sensors currently do not produce data or do not upload it to the Raspberry Shake database. An ongoing relationship between community organizations and scientists can ensure that the sensors remain connected and in working order, and that communities are able to benefit educationally by getting involved in research projects. This has the added benefit of increasing awareness of geoscience and encouraging children to explore this field in the future.

A less involved and shorter-term study would involve placing a line of seismic nodes at regular intervals starting at a frequent source of seismic activity such as a quarry. Active quarries are common throughout the Piedmont (at least 6 are located in Maryland), and individual quarries generally conduct blasting anywhere from several times a week to several times a month meaning that the nodes would only need to be deployed for around a month. These quarry blasts are detectable by existing Raspberry Shake stations at distances of up to 33 km. First arrival times for P-waves as well as P-S wave time differences could be used to construct a 1-dimensional velocity model extending down to around 11 km (based on the rough rule that depth resolution is about $1/3$ of the seismic line length). Such a study could be constructed at essentially no cost by research institutions that possess seismic nodes. Multiple studies in different directions could be conducted to gain an approximate knowledge of the 3-dimensional velocity structure.

Finally active source seismic reflection studies could be conducted near the location of suspected shallow faults to image these faults. This could produce high resolution maps of faults, which could be used to inform engineering and geological injection (waste-disposal, carbon capture and storage) projects.

Even without the help of the above scientific wish-list, the moment tensor solution can be tested by using it to produce waveforms for the 6/27/21 and 8/15/21 Baltimore earthquakes, which may be aftershocks of the 6/25/21 event and may have occurred along the same fault system. If so, the 6/25/21 moment tensor found by this research should fit the waveforms from the aftershocks. A more involved approach would be to independently find the moment tensors for each of these events and compare them. Finding moment tensors for other earthquakes throughout Maryland, Virginia, Pennsylvania, and New Jersey would contribute significantly to knowledge of the stress field in this region and would shed light on local vs. regional stress fields in intraplate areas and how they contribute to seismicity.

CONCLUSION AND BROADER IMPLICATIONS

Moment tensor inversion was used to produce a stable focal mechanism for an earthquake that occurred on June 25th, 2021 in Baltimore, Maryland. The results indicated a normal faulting mechanism on a fault oriented at either $148^{\circ} \pm 15^{\circ}$ or $281^{\circ} \pm 4^{\circ}$ and a maximum tensile stress acting at $-135^{\circ} \pm 4^{\circ}$ azimuth (NE-SW). Given that the regional stress field is compressional with maximum compressional stress acting E-W to NE-SW, the results suggest the existence of an anomalous local stress field. However, the numerous sources of error involved in the inversion mean that the results should be treated with caution and ideally should be replicated using a technique better suited to sampling the entire space of parameters. Further research should focus on improving seismic velocity models and finding focal mechanisms for other earthquakes throughout the mid-Atlantic region.

Moment tensor inversion for small earthquakes in the eastern United States can provide valuable information about the stress field and how it relates to seismicity. This can help us better evaluate local seismic hazards and may also shed light on the general behavior of stress in intraplate regions such as the New Madrid Seismic Zone and the Tianshan region of China, the source of 6 of the 10 deadliest earthquakes in recorded history (Kusky et al, 2007). If the current results of this research are confirmed, it would indicate that small scale seismicity is driven by local anomalous fields. These fields might help redistribute stress in Maryland and Northern Virginia and explain why stress becomes concentrated in other regions, such as the Central Virginia Seismic Zone and the region around Charleston, SC (the location of a deadly earthquake in 1886). While this is speculation, it nevertheless underscores the importance of investigating these questions: the reasons for stress accumulation in intraplate regions is poorly understood. Insights may be gained not just by studying the locations of known severe intraplate earthquakes, but also by studying regions where more gentle seismicity occurs for equally unclear reasons.

ACKNOWLEDGEMENTS

I would like to thank my advisor Ved Lekic for being such an amazing support during this project. I would also like to thank Phil Piccoli, Karen Prestegard, Nick Schmerr, Wenlu Zhu, Alex Lastner, Ashley Hannah, & Ben Moyer for their valuable suggestions, technical assistance, and encouragement in difficult times. For personal assistance and sound advice, I am infinitely indebted to my sweet girlfriend, Gray, and to my friends Howard, Annice, and Alan.

BIBLIOGRAPHY

Allen, C. R. (1975). Geological Criteria for Evaluating Seismicity Address as Retiring President of The Geological Society of America, Miami Beach, Florida, November 1974. *GSA Bulletin*, 86(8), 1041–1057.

Allmendinger, R. W., Cardozo, N. C., and Fisher, D. (2013). Structural Geology Algorithms: Vectors & Tensors: Cambridge, England, Cambridge University Press, 289 pp.

- Bollinger, G. A. (1969). Seismicity of the central Appalachian states of Virginia, West Virginia, and Maryland—1758 through 1968. *Bulletin of the Seismological Society of America*, 59(5), 2103–2111. <https://doi.org/10.1785/bssa0590052103>
- Bollinger, G. A. (1973). Seismicity of the southeastern United States. *Bulletin of the Seismological Society of America*, 63(5), 1785–1808. <https://doi.org/10.1785/bssa0630051785>
- Bollinger, G., Chapman, M., & Moore, T. (1980). *Seismic velocity structure of central Virginia* (NUREG/CR-1217, pp.1-133.). Central Virginia Regional Seismic Network. <https://www.osti.gov/scitech/biblio/5499803-central-virginia-regional-seismic-network-crustal-velocity-structure-central-southwestern-virginia-compute-epicentral-distance-surface-velocity-function-azimuth-fortran-ibm>
- Brocher, T. M. (2005). Empirical Relations between Elastic Wavespeeds and Density in the Earth's Crust. *Bulletin of the Seismological Society of America*, 95(6), 2081–2092. <https://doi.org/10.1785/0120050077>
- Chapman, M. C. (2013). On the Rupture Process of the 23 August 2011 Virginia Earthquake. *Bulletin of the Seismological Society of America*, 103(2A), 613–628. <https://doi.org/10.1785/0120120229>
- Cleaves, E. T., Jonathan Jr., E., & J.D., G. (1968). *Geologic map of Maryland* [Map]. Maryland Geological Survey.
- Crowley, W., Reinhardt, J., & Cleaves, E. (1976). *Geologic map of Baltimore County and City* [Map].
- Drake, A., Jr. (1994). The Soldiers Delight Ultramafite in the Maryland Piedmont. *U.S. Geological Survey Bulletin*, 2076.
- Drake, A. A. (1998). Geologic map of the Piedmont in the Savage and Relay quadrangles, Howard, Baltimore, and Anne Arundel Counties, Maryland. *Open-File Report (United States Geological Survey. 1978), Open File Report 98-757*. <https://doi.org/10.3133/ofr98757>
- Du, W., Kim, Y.-J., & Sykes, L. R. (2003). Earthquake Source Parameters and State of Stress for the Northeastern United States and Southeastern Canada from Analysis of Regional Seismograms. *Bulletin of the Seismological Society of America*, 93(4), 1633–1648. <https://doi.org/10.1785/0120020217>
- Ekström, G. (2017). Short-period surface-wave phase velocities across the conterminous United States. *Physics of the Earth and Planetary Interiors*, 270, 168–175. <https://doi.org/10.1016/j.pepi.2017.07.010>

- Gaherty, J. B., Dalton, C., & Levin, V. (2009). *Three-dimensional models of crustal structure in eastern North America, Final Technical Report* (USGS NEHRP Grant 07HQGR0046). USGS.
- Guo, W., Zhao, S., Wang, F., Yang, Z., Jia, S., & Liu, Z. (2019). Crustal structure of the eastern Piedmont and Atlantic coastal plain in North Carolina and Virginia, eastern North American margin. *Earth, Planets and Space*, 71(1). <https://doi.org/10.1186/s40623-019-1049-z>
- Herrmann, R. B. (1979). Surface wave focal mechanisms for eastern North American earthquakes with tectonic implications. *Journal of Geophysical Research: Solid Earth*, 84(B7), 3543–3552. <https://doi.org/10.1029/jb084ib07p03543>
- Heidbach, O., Rajabi, M., Cui, X., Fuchs, K., Müller, B., Reinecker, J., Reiter, K., Tingay, M., Wenzel, F., Xie, F., Ziegler, M. O., Zoback, M.-L., & Zoback, M. (2018). The World Stress Map database release 2016: Crustal stress pattern across scales. *Tectonophysics*, 744(Technical Report 16-01), 484–498. <https://doi.org/10.1016/j.tecto.2018.07.007>
- Heimann, Sebastian; Kriegerowski, Marius; Isken, Marius; Cesca, Simone; Daout, Simon; Grigoli, Francesco; Juretzek, Carina; Megies, Tobias; Nooshiri, Nima; Steinberg, Andreas; Sudhaus, Henriette; Vasyura-Bathke, Hannes; Willey, Timothy; Dahm, Torsten (2017): Pyrocko - An open-source seismology toolbox and library. V. 0.3. GFZ Data Services. <https://doi.org/10.5880/GFZ.2.1.2017.001>
- Horton, J.W., Jr., Chapman, M.C., Carter, A.M., Carter, M.W., Harrison, R.W., Herrmann, R.B., and Snyder, S.L., 2012a, Faults delineated by after- shocks associated with the 2011 central Virginia earthquake and their tectonic setting: Geological Society of America Abstracts with Programs, v. 44, no. 4, p. 14.
- Horton, J. W., Chapman, M. C., & Green, R. A. (2015). The 2011 Mineral, Virginia, earthquake, and its significance for seismic hazards in eastern North America—Overview and synthesis. *The 2011 Mineral, Virginia, Earthquake, and Its Significance for Seismic Hazards in Eastern North America, Special Paper 509*. [https://doi.org/10.1130/2015.2509\(01\)](https://doi.org/10.1130/2015.2509(01))
- Horton, J.W., Jr., McNamara, D.E., Shah, A.K., Gilmer, A.K., Carter, A.M., Burton, W.C., Harrison, R.W., Carter, M.W., Herrmann, R.B., and Snyder, S.L., 2012b, Preliminary analysis of magnitude 5.8 Virginia Earthquake causative fault and subsidiary faults illuminated by aftershocks: Geological Society of America Abstracts with Programs, v. 44, no. 7, p. 381.
- Hough, S. E., & Bilham, R. G. (2006). *After the earthquakes: elastic rebound on an urban planet*. Oxford University Press.

- James, D. E., Smith, T. J., & Steinhart, J. S. (1968). Crustal structure of the Middle Atlantic states. *Journal of Geophysical Research Atmospheres*, 73(6), 1983–2007. <https://doi.org/10.1029/jb073i006p01983>
- Jost, M. L., & Hermann, R. B. (1989). A Student's Guide to and Review of Moment Tensors. *Seismological Research Letters*, 60(2), 37-57
- Kim, W., Gold, M., Ramsay, J., Meltzer, A., Wunsch, D. R., Baxter, Lekic, V., S. J., Lognonné, P., Goodling, P. J., Pearson, K. M., Wagner, L. S., Roman, D. C., & Pratt, T. L. (2018). The MW 4.2 Delaware earthquake of 30 November 2017. *Seismological Research Letters*, 89(6), 2447–2460. <https://doi.org/10.1785/0220180124>
- Kuang, J., Long, L. T., & Mareschal, J.-C. (1989). Intraplate seismicity and stress in the southeastern United States. *Tectonophysics*, 170(1-2), 29–42. [https://doi.org/10.1016/0040-1951\(89\)90101-7](https://doi.org/10.1016/0040-1951(89)90101-7)
- Kusky, T. M., Windley, B. F., & Zhai, M. (n.d.). Tectonic evolution of the North China Block: From orogen to craton to orogen. *Geological Society London Special Publications*, 280(1), 1–34. <https://doi.org/10.1144/sp280.1>
- Levandowski, W., Herrmann, R. B., Briggs, R., Boyd, O., & Gold, R. (2018). An updated stress map of the continental United States reveals heterogeneous intraplate stress. *Nature Geoscience*, 11(6), 433–437. <https://doi.org/10.1038/s41561-018-0120-x>
- Lundstern, J.-E., & Zoback, M. D. (2023). Multiscale variations of the crustal stress field throughout North America. *Nature Communications*, 14(1). <https://doi.org/10.1038/s41467-022-34915-0>
- Magrini, F. (2023). BayesBay [Source code]. GitHub <https://github.com/fmagrini/bayes-bay/tree/main>
- Maguire, R., V. Lekić, Kim, D., N. Schmerr, Li, J., C. Beghein, Huang, Q., Irving, F. Karakostas, P. Lognonné, Stähler, S. C., & Banerdt, W. B. (2023). Focal Mechanism Determination of Event S1222a and Implications for Tectonics Near the Dichotomy Boundary in Southern Elysium Planitia, Mars. *Journal of Geophysical Research. Planets (Print)*, 128(9). <https://doi.org/10.1029/2023je007793>
- Mooney, & Boyd, O. S. (2021). *Database of Central and Eastern North American Seismic Velocity Structure* [Dataset]. U.S. Geological Survey. <https://doi.org/10.5066/P91620O4>. <https://www.sciencebase.gov/catalog/item/608805a2d34e0fbbe3ddb82d>
- Munsey, J. W., & Bollinger, G. A. (1985). Focal mechanism analyses for Virginia earthquakes (1978-1984). *Bulletin of the Seismological Society of America*, 75(6), 1613–1636. <https://doi.org/10.1785/bssa0750061613>
- Nyblade, A., & Homman, K. (2016). *Seismicity in Pennsylvania from February 2013 to June 2015: Report submitted to the State Geologist and Director of the Bureau of Topographic*

- and Geologic Survey, Department of Conservation and Natural Resources. Pennsylvania State Seismic Network. <http://paseis.geosc.psu.edu/Report/PASEISReport.pdf>.
- O'Toole, T. B., & Woodhouse, J. H. (2011). Numerically stable computation of complete synthetic seismograms including the static displacement in plane layered media. *Geophysical Journal International*, 187(3), 1516–1536. <https://doi.org/10.1111/j.1365-246x.2011.05210.x>
- Peterson, M., Moschetti, M., & Haller, K. (2014). The 2014 U.S. National Seismic Hazard Maps: A summary of changes to seismic source and ground motion models. *Tenth U.S. National Conference on Earthquake Engineering Frontiers of Earthquake Engineering*. <https://doi.org/10.4231/D3MS3K254>
- Reger, J., & Maryland Geological Survey. (1987). *Earthquakes and Maryland*. Wwww.mgs.md.gov. http://www.mgs.md.gov/geology/geohazards/earthquakes_and_maryland.html
- Sheridan, R. E., Olsson, R. K., & Miller, J. J. (1991). Seismic reflection and gravity study of proposed Taconic suture under the New Jersey Coastal Plain: Implications for continental growth. *Geological Society of America Bulletin*, 103(3), 402–414. [https://doi.org/10.1130/0016-7606\(1991\)103](https://doi.org/10.1130/0016-7606(1991)103)
- Shearer, P. M. (2019). *Introduction to Seismology*. Cambridge University Press.
- Soto-Cordero, L., Meltzer, A., & Stachnik, J. C. (2017). Crustal Structure, Intraplate Seismicity, and Seismic Hazard in the Mid-Atlantic United States. *Seismological Research Letters*, 89(1), 241–252. <https://doi.org/10.1785/0220170084>
- Surprise! Maryland area shakes with quakes. (1993, April 4). *The New York Times*, 28.
- USGS Earthquake Hazards Program. (2019). *Earthquakes in Eastern U.S. | U.S. Geological Survey*. www.usgs.gov. Retrieved April 19, 2024, from <https://www.usgs.gov/media/images/earthquakes-eastern-us>
- USGS National Earthquakes Information Center. (2024, April 5). *M 4.8 - 2024 Tewksbury, New Jersey Earthquake*. Usgs.gov. <https://earthquake.usgs.gov/earthquakes/eventpage/at00sbh3yv/moment-tensor>
- Valentine, A. (2022). Pyprop8 [Source code]. GitHub. <https://github.com/valentineap/pyprop8/tree/master>
- Vavryčuk, V. (2015). Moment Tensors: Decomposition and Visualization. *Encyclopedia of Earthquake Engineering*, 1–16. https://doi.org/10.1007/978-3-642-36197-5_288-1

- Viegas, G. (2012). Source Parameters of the 16 July 2010 Mw 3.4 Germantown, Maryland, Earthquake. *Seismological Research Letters*, 83(5), 933–944.
<https://doi.org/10.1785/0220110056>
- Walsh, L. (2013). *The Tectonics of intraplate regions: quantifying stress and surface deformations in the central and eastern U.S. and planetary analogs on Mercury and the moon*. (2013). [PhD Dissertation]. University of Maryland.
- Whitney Barlow Robles. (2017). Atlantic Disaster: Boston Responds to the Cape Ann Earthquake of 1755. *The New England Quarterly*, 90(1).
https://doi.org/10.1162/tneq_a_00583
- WUSA9 News. (2024, January 2). *Rare 2.3 magnitude earthquake hits Rockville, Maryland*. Wwww.youtube.com. <https://www.youtube.com/watch?v=IoiJ1hVSuvM>
- Yang, J.-P., & Aggarwal, Y. P. (1981). Seismotectonics of northeastern United States and adjacent Canada. *Journal of Geophysical Research: Solid Earth*, 86(B6), 4981–4998.
<https://doi.org/10.1029/jb086ib06p04981>
- Zoback, M. L. (1992). Stress field constraints on intraplate seismicity in eastern North America. *Journal of Geophysical Research*, 97(B8), 11761.
<https://doi.org/10.1029/92jb00221>
- Zoback, M. L., & Zoback, M. D. (1989). Chapter 24: Tectonic stress field of the continental United States. In *Memoir - Geological Society of America* (pp. 523–540). <https://doi.org/10.1130/mem172-p523>

APPENDIX A: Velocity models referenced

All models except the Test Model and those by Chapman (2013) and Nyblade and Homman (2016) were compiled by Mooney and Boyd (2021) in a database of 1-D models for the Central and Eastern United States.

Velocity Units: km/s Thickness/Depth Units: km

MODELS USED IN THE INVERSION

Location Name: Charlottesville E1

Coordinates: (37.97, -78.11)

Source: Chapman (2013)

| V_p | V_s | Thickness | Layer Top |
|-------|-------|-----------|-----------|
| 6.09 | 3.53 | 15 | 0 |
| 6.5 | 3.79 | 21 | 15 |
| 8.18 | 4.73 | infinite | 36 |

Location Name: Richmond E

Coordinates: (37.7, -77.89)

Source: Munsey & Bollinger (1985)

| V_p | V_s | Thickness | Layer Top |
|-------|-------|-----------|-----------|
| 6.09 | 3.52 | 18 | 0 |
| 6.67 | 3.86 | 18 | 18 |
| 8.18 | 4.73 | infinite | 36 |

Location Name: SE Pennsylvania

Coordinates: N/A

Source: Nyblade and Homman (2016)

| V_p | V_s | Thickness | Layer Top |
|-------|-------|-----------|-----------|
| 6 | | 10 | 0 |
| 6.3 | | 10 | 10 |
| 6.6 | | 10 | 20 |
| 6.9 | | 7 | 30 |
| 8.1 | | infinite | 37 |

Location Name: Test Model
Coordinates: N/A
Source: Yuval Ravinsky-Gray

| V_p | V_s | Thickness | Layer Top |
|-------|-------|-----------|-----------|
| 5.2 | | 0.2 | 0 |
| 5.5 | | 0.2 | 0.2 |
| 5.3 | | 0.2 | 0.4 |
| 5.6 | | 0.2 | 0.6 |
| 5.8 | | 0.2 | 0.8 |
| 6 | | 0.5 | 1 |
| 6.1 | | 9.5 | 1.5 |
| 6.2 | | 5 | 10 |
| 6.3 | | 3 | 15 |
| 6.4 | | 2 | 18 |
| 6.5 | | 10 | 20 |
| 6.6 | | 5 | 30 |
| 6.7 | | 1 | 35 |
| 8.15 | | infinite | 36 |

OTHER MODELS

Location Name: Charlottesville W
Coordinates: (38.1, -78.53)
Source: Bollinger et al. (1980)

| V_p | V_s | Thickness | Layer Top |
|-------|-------|-----------|-----------|
| 6.09 | 3.53 | 15 | 0 |
| 6.5 | 3.79 | 24 | 15 |
| 8.18 | 4.73 | infinite | 39 |

Location Name: Millville (NJ)

Coordinates: (39.41, -74.9)

Source: Sheridan et al. (1991)

| V_p | V_s | Thickness | Layer Top |
|-------|-------|-----------|-----------|
| 2.05 | | 0.43 | 0 |
| 2.75 | | 0.68 | 0.43 |
| 4.5 | | 1.2 | 1.11 |
| 5.3 | | 1.18 | 2.31 |
| 5.9 | | 4.56 | 3.49 |
| 6.1 | | infinite | 8.05 |

Location Name: Ocean City (NJ)

Coordinates: (39.25, -74.75)

Source: Gaherty et al. (2009)

| V_p | V_s | Thickness | Layer Top |
|-------|-------|-----------|-----------|
| 2.74 | 1.58 | 3.7 | 0 |
| 6.44 | 3.72 | 26.3 | 3.7 |
| 6.58 | 3.8 | 2.6 | 30 |

Location Name: Silver Spring

Coordinates: (39, -77)

Source: James et al. (1968)

| V_p | V_s | Thickness | Layer Top |
|-------|-------|-----------|-----------|
| 6.5 | | 34 | 0 |
| 8.15 | | infinite | 34 |

Location Name: Charlottesville E2

Coordinates: (37.89, -78.26)

Source: Bollinger et al. (1980)

| V_p | V_s | Thickness | Layer Top |
|-------|-------|-----------|-----------|
| 5.62 | | 2 | 0 |
| 6.09 | | ? | 2 |

Location Name: Richmond W
Coordinates: (37.71, -77.87)
Source: Bollinger et al. (1980)

| V_p | V_s | Thickness | Layer Top |
|-------|-------|-----------|-----------|
| 5.62 | | 0.7 | 0 |
| 6.09 | | ? | 0.7 |

APPENDIX B: Code for moment tensor inversion

Inversion code for Baltimore 6/25/21 earthquake using the Chapman (2013) model. The codes for the other models are identical apart from the model input.

Written by Yuval Ravinsky-Gray.

PART 1: Data input and processing

```
# Multistation Inversion without rotation
# Baltimore
# 39.3043°N 76.7078°W
# 2.5 km depth ?
# 6/25/2021
# Magnitude: Mb_Lg 2.6
# Stations: SDMD, SUDB, FMMC, WUPA, REST, R0ECF, RAD82

Nsta = 7

Ncomp = 3

import pyprop8 as pp
from pyprop8.utils import
rtf2xyz,make_moment_tensor,stf_trapezoidal,stf_cosine,latlon2xy,stf_boxcar,stf_cosine_boxcar
import numpy as np
import matplotlib.pyplot as plt
import obspy.signal.filter
import scipy
from scipy import signal
import obspy.imaging.beachball
from obspy import read
from scipy import interpolate
from obspy.clients.fdsn import Client
from obspy import UTCDateTime
```

```
#####
##### Set spacing and bounds of inversion #####
#####

# Filter (upper limit must be lower than Nyquist)
# Nyquist freq = 5 Hz
# decimate every 10th value
# New sampling rate = 10 Hz
# Period = 0.1 s
# original length = 1201
# new length (nt) = 1200

delta_t = 0.1 # DESIRED sampling interval (used in synthetic calculations)
print('dt = ', delta_t)
print(' ')

nt = 500
print('nt = ', nt)
print(' ')

# make data array for all stations
seismograms = np.zeros(shape=(Nsta,Ncomp,nt))

#####
##### BAND PASS FILTERING REQUIRED FOR DECIMATION
#####
data_delta_t = 0.01 # ACTUAL delta t for the data
# Filter (upper limit must be lower than Nyquist)
sos = signal.butter(4, [0.5, 1], btype='bandpass', analog=False, output='sos', fs=1/data_delta_t)

#####
##### Input Station Data #####
#####

# Import SDMD Data (1)
SDMD_E = read('SDMD.LD..HHE.2021.176.19.40.45.000-2021.176.19.42.45.000.rm.correct.t-
0.0001-0.0002-19-20.miniseed')
E1 = SDMD_E[0].data
SDMD_N = read('SDMD.LD..HHN.2021.176.19.40.45.000-2021.176.19.42.45.000.rm.correct.t-
0.0001-0.0002-19-20.miniseed')
N1 = SDMD_N[0].data
SDMD_Z = read('SDMD.LD..HHZ.2021.176.19.40.45.000-2021.176.19.42.44.999.rm.correct.t-
0.0001-0.0002-19-20.miniseed')
```

```

Z1 = SDMD_Z[0].data

E11 = signal.sosfilt(sos, E1)
N11 = signal.sosfilt(sos, N1)
Z11 = signal.sosfilt(sos, Z1)

##### interpolation for data -- this allows you to shift #####

# time_des = desired time vector (same as time synthetics are calculated )
time_des = delta_t*np.arange(0,nt,1) # this is our desired time vector --> should be the same as
the time vector of the synthetics

# below, for time_data make delta_t = 0.01 for 100 Hz data

time_dataE1 = data_delta_t*np.arange(0,len(E11),1) # this is the time of the input data
tmp_intrpE1 = interpolate.interp1d(time_dataE1,E11,kind='linear',fill_value='extrapolate')
seismograms[0,0,:] = tmp_intrpE1(time_des)
# time_data - phase shift

time_dataN1 = data_delta_t*np.arange(0,len(N11),1) # this is the time of the input data
tmp_intrpN1 = interpolate.interp1d(time_dataN1,N11,kind='linear',fill_value='extrapolate')
seismograms[0,1,:] = tmp_intrpN1(time_des)

time_dataZ1 = data_delta_t*np.arange(0,len(Z11),1) # this is the time of the input data
tmp_intrpZ1 = interpolate.interp1d(time_dataZ1,Z11,kind='linear',fill_value='extrapolate')
seismograms[0,2,:] = tmp_intrpZ1(time_des)

#####

# Import SUDB Data (2)
SUDB_E = read('SUDB.4P..HHE.2021.176.19.40.45.000-2021.176.19.42.45.000.rm.correct.t-
0.0001-0.0002-19-20.miniseed')
E2 = SUDB_E[0].data
SUDB_N = read('SUDB.4P..HHN.2021.176.19.40.45.000-2021.176.19.42.45.000.rm.correct.t-
0.0001-0.0002-19-20.miniseed')
N2 = SUDB_N[0].data
SUDB_Z = read('SUDB.4P..HHZ.2021.176.19.40.45.000-2021.176.19.42.44.999.rm.correct.t-
0.0001-0.0002-19-20.miniseed')
Z2 = SUDB_Z[0].data

E22 = signal.sosfilt(sos, E2)
N22 = signal.sosfilt(sos, N2)
Z22 = signal.sosfilt(sos, Z2)

##### interpolation for data -- this allows you to shift #####

```

```

time_dataE2 = data_delta_t*np.arange(0,len(E22),1) # this is the time of the input data
tmp_intrpE2 = interpolate.interp1d(time_dataE2,E22,kind='linear',fill_value='extrapolate')
seismograms[1,0,:] = tmp_intrpE2(time_des)

time_dataN2 = data_delta_t*np.arange(0,len(N22),1) # this is the time of the input data
tmp_intrpN2 = interpolate.interp1d(time_dataN2+.2,N22,kind='linear',fill_value='extrapolate')
seismograms[1,1,:] = tmp_intrpN2(time_des)

time_dataZ2 = data_delta_t*np.arange(0,len(Z22),1) # this is the time of the input data
tmp_intrpZ2 = interpolate.interp1d(time_dataZ2,Z22,kind='linear',fill_value='extrapolate')
seismograms[1,2,:] = tmp_intrpZ2(time_des)

#####

# Import FMMC Data (3)
FMMC_E = read('FMMC.LD..HHE.2021.176.19.40.45.000-2021.176.19.42.45.000.rm.correct.t-
0.0001-0.0002-19-20.miniseed')
E3 = FMMC_E[0].data
FMMC_N = read('FMMC.LD..HHN.2021.176.19.40.45.000-
2021.176.19.42.44.999.rm.correct.t-0.0001-0.0002-19-20.miniseed')
N3 = FMMC_N[0].data
FMMC_Z = read('FMMC.LD..HHZ.2021.176.19.40.45.000-2021.176.19.42.45.000.rm.correct.t-
0.0001-0.0002-19-20.miniseed')
Z3 = FMMC_Z[0].data

E33 = signal.sosfilt(sos, E3)
N33 = signal.sosfilt(sos, N3)
Z33 = signal.sosfilt(sos, Z3)

##### interpolation for data -- this allows you to shift #####

time_dataE3 = data_delta_t*np.arange(0,len(E33),1) # this is the time of the input data
tmp_intrpE3 = interpolate.interp1d(time_dataE3,E33,kind='linear',fill_value='extrapolate')
seismograms[2,0,:] = tmp_intrpE3(time_des)

time_dataN3 = data_delta_t*np.arange(0,len(N33),1) # this is the time of the input data
tmp_intrpN3 = interpolate.interp1d(time_dataN3+.7,N33,kind='linear',fill_value='extrapolate')
seismograms[2,1,:] = tmp_intrpN3(time_des)

time_dataZ3 = data_delta_t*np.arange(0,len(Z33),1) # this is the time of the input data
tmp_intrpZ3 = interpolate.interp1d(time_dataZ3-3.2,Z33,kind='linear',fill_value='extrapolate')
seismograms[2,2,:] = tmp_intrpZ3(time_des)

```

```
#####
```

```
# Import WUPA Data (4)
WUPA_E = read('WUPA.LD..HHE.2021.176.19.40.45.005-2021.176.19.42.44.995.rm.correct.t-
0.0001-0.0002-19-20.miniseed')
E4 = WUPA_E[0].data
WUPA_N = read('WUPA.LD..HHN.2021.176.19.40.45.005-2021.176.19.42.44.995.rm.correct.t-
0.0001-0.0002-19-20.miniseed')
N4 = WUPA_N[0].data
WUPA_Z = read('WUPA.LD..HHZ.2021.176.19.40.45.005-2021.176.19.42.44.994.rm.correct.t-
0.0001-0.0002-19-20.miniseed')
Z4 = WUPA_Z[0].data
print(len(E4))
E44 = signal.sosfilt(sos, E4)
N44 = signal.sosfilt(sos, N4)
Z44 = signal.sosfilt(sos, Z4)
```

```
time_dataE4 = data_delta_t*np.arange(0,len(E44),1) # this is the time of the input data
tmp_intrapE4 = interpolate.interpld(time_dataE4-.3,E44,kind='linear',fill_value='extrapolate')
seismograms[3,0,:] = tmp_intrapE4(time_des)
```

```
time_dataN4 = data_delta_t*np.arange(0,len(N44),1) # this is the time of the input data
tmp_intrapN4 = interpolate.interpld(time_dataN4-1.2,N44,kind='linear',fill_value='extrapolate')
seismograms[3,1,:] = tmp_intrapN4(time_des)
```

```
time_dataZ4 = data_delta_t*np.arange(0,len(Z44),1) # this is the time of the input data
tmp_intrapZ4 = interpolate.interpld(time_dataZ4-2.7,Z44,kind='linear',fill_value='extrapolate')
seismograms[3,2,:] = tmp_intrapZ4(time_des)
```

```
#####
```

```
# Import REST Data (5)
REST_E = read('REST.4P..HHE.2021.176.19.40.45.000-2021.176.19.42.44.999.rm.correct.t-
0.0001-0.0002-19-20.miniseed')
E5 = REST_E[0].data
REST_N = read('REST.4P..HHN.2021.176.19.40.45.000-2021.176.19.42.45.000.rm.correct.t-
0.0001-0.0002-19-20.miniseed')
N5 = REST_N[0].data
REST_Z = read('REST.4P..HHZ.2021.176.19.40.45.000-2021.176.19.42.44.999.rm.correct.t-
0.0001-0.0002-19-20.miniseed')
Z5 = REST_Z[0].data
```

```
E55 = signal.sosfilt(sos, E5)
N55 = signal.sosfilt(sos, N5)
N55[0:1000] = 0 # remove artifact from filtering
Z55 = signal.sosfilt(sos, Z5)
```

```

time_dataE5 = data_delta_t*np.arange(0,len(E55),1) # this is the time of the input data
tmp_intrpE5 = interpolate.interp1d(time_dataE5-.2,E55,kind='linear',fill_value='extrapolate')
seismograms[4,0,:] = tmp_intrpE5(time_des)

time_dataN5 = data_delta_t*np.arange(0,len(N55),1) # this is the time of the input data
tmp_intrpN5 = interpolate.interp1d(time_dataN5,N55,kind='linear',fill_value='extrapolate')
seismograms[4,1,:] = tmp_intrpN5(time_des)

time_dataZ5 = data_delta_t*np.arange(0,len(Z55),1) # this is the time of the input data
tmp_intrpZ5 = interpolate.interp1d(time_dataZ5-1,Z55,kind='linear',fill_value='extrapolate')
seismograms[4,2,:] = tmp_intrpZ5(time_des)

#####

# Import R0ECF Data (6)
start_1 = "2021-06-25 19:40:00"
starttime = UTCDateTime(start_1)
endtime = starttime + 165 # 165 seconds (45 extra seconds to get rid of artifact at beginning)
client = Client(base_url='https://data.raspberrypi.org/')

R0ECF_E = client.get_waveforms('AM', 'R0ECF', '00', 'EHE', starttime, endtime)
E6 = R0ECF_E[0].data/1e9
R0ECF_N = client.get_waveforms('AM', 'R0ECF', '00', 'EHN', starttime, endtime)
N6 = R0ECF_N[0].data/1e9
R0ECF_Z = client.get_waveforms('AM', 'R0ECF', '00', 'EHZ', starttime, endtime)
Z6 = R0ECF_Z[0].data/1e9

E66A = signal.sosfilt(sos, E6)
N66A = signal.sosfilt(sos, N6)
Z66A = signal.sosfilt(sos, Z6)

# Remove extra time at beginning
E66 = E66A[4500:16500]
N66 = N66A[4500:16500]
Z66 = Z66A[4500:16500]

time_dataE6 = data_delta_t*np.arange(0,len(E66),1) # this is the time of the input data
tmp_intrpE6 = interpolate.interp1d(time_dataE6,E66,kind='linear',fill_value='extrapolate')
seismograms[5,0,:] = tmp_intrpE6(time_des)

time_dataN6 = data_delta_t*np.arange(0,len(N66),1) # this is the time of the input data
tmp_intrpN6 = interpolate.interp1d(time_dataN6,N66,kind='linear',fill_value='extrapolate')
seismograms[5,1,:] = tmp_intrpN6(time_des)

time_dataZ6 = data_delta_t*np.arange(0,len(Z66),1) # this is the time of the input data

```

```

tmp_intrpZ6 = interpolate.interp1d(time_dataZ6,Z66,kind='linear',fill_value='extrapolate')
seismograms[5,2,:] = tmp_intrpZ6(time_des)

#####

# Import RAD82 Data (7)
# only one channel: make zero vectors for others
start_1 = "2021-06-25 19:40:00"
starttime = UTCDateTime(start_1)
endtime = starttime + 165 # 165 seconds (45 extra seconds to get rid of artifact at beginning)
RAD82_Z = client.get_waveforms('AM', 'RAD82', '00', 'EHZ', starttime, endtime)
Z7 = RAD82_Z[0].data/1e9

Z77A = signal.sosfilt(sos, Z7)

# Remove extra time at beginning
Z77 = Z77A[4500:16500]

# make zero vectors for E and N components
E77 = np.zeros(len(Z77))
N77 = np.zeros(len(Z77))

time_dataE7 = data_delta_t*np.arange(0,len(E77),1) # this is the time of the input data
tmp_intrpE7 = interpolate.interp1d(time_dataE7,E77,kind='linear',fill_value='extrapolate')
seismograms[6,0,:] = tmp_intrpE7(time_des)

time_dataN7 = data_delta_t*np.arange(0,len(N77),1) # this is the time of the input data
tmp_intrpN7 = interpolate.interp1d(time_dataN7,N77,kind='linear',fill_value='extrapolate')
seismograms[6,1,:] = tmp_intrpN7(time_des)

time_dataZ7 = data_delta_t*np.arange(0,len(Z77),1) # this is the time of the input data
tmp_intrpZ7 = interpolate.interp1d(time_dataZ7-2,Z77,kind='linear',fill_value='extrapolate') #
+.4
seismograms[6,2,:] = tmp_intrpZ7(time_des) # This should shift earlier by 1 s

```

Part 2: Plot Waveforms for original data and interpolated data

Plot waveforms for original data and interpolation

```

fig = plt.figure(figsize=(12,3*Nsta))
fig.suptitle('Comparison of Waveforms and Inversion for Baltimore
6/25/21',fontsize='18',fontweight='bold')

```

```

# station 1 (SDMD)

```

```

ax = fig.add_subplot(Nsta,Ncomp,1)
ax.plot(time_dataE1[0:nt*10],E11[0:nt*10],'blue',label='raw data')
ax.plot(time_des, seismograms[0,0,:],'red',label='interpolation')
ax.set_title('East',fontsize='14',fontweight='bold')
ax.set_ylabel('SDMD',fontsize='14',fontweight='bold')
ax.set_xlim(0,nt*delta_t)
ax.legend()

ax = fig.add_subplot(Nsta,Ncomp,2)
ax.plot(time_dataN1[0:nt*10],N11[0:nt*10],'blue',label='raw data')
ax.plot(time_des, seismograms[0,1,:],'red',label='interpolation')
ax.set_title('North',fontsize='14',fontweight='bold')
ax.set_xlim(0,nt*delta_t)

ax = fig.add_subplot(Nsta,Ncomp,3)
ax.plot(time_dataZ1[0:nt*10],Z11[0:nt*10],'blue',label='raw data')
ax.plot(time_des, seismograms[0,2,:],'red',label='interpolation')
ax.set_title('Vertical',fontsize='14',fontweight='bold')
ax.set_xlim(0,nt*delta_t)

# station 2 (SUDB)
ax = fig.add_subplot(Nsta,Ncomp,4)
ax.plot(time_dataE2[0:nt*10],E22[0:nt*10],'blue',label='raw data')
ax.plot(time_des, seismograms[1,0,:],'red',label='interpolation')
ax.set_title('East',fontsize='14',fontweight='bold')
ax.set_ylabel('SUDB',fontsize='14',fontweight='bold')
ax.set_xlim(0,nt*delta_t)

ax = fig.add_subplot(Nsta,Ncomp,5)
ax.plot(time_dataN2[0:nt*10],N22[0:nt*10],'blue',label='raw data')
ax.plot(time_des, seismograms[1,1,:],'red',label='interpolation')
ax.set_title('North',fontsize='14',fontweight='bold')
ax.set_xlim(0,nt*delta_t)

ax = fig.add_subplot(Nsta,Ncomp,6)
ax.plot(time_dataZ2[0:nt*10],Z22[0:nt*10],'blue',label='raw data')
ax.plot(time_des, seismograms[1,2,:],'red',label='interpolation')
ax.set_title('Vertical',fontsize='14',fontweight='bold')
ax.set_xlim(0,nt*delta_t)

# station 3 (FMMC)
ax = fig.add_subplot(Nsta,Ncomp,7)
ax.plot(time_dataE3[0:nt*10],E33[0:nt*10],'blue',label='raw data')
ax.plot(time_des, seismograms[2,0,:],'red',label='interpolation')
ax.set_title('East',fontsize='14',fontweight='bold')
ax.set_ylabel('FMMC',fontsize='14',fontweight='bold')

```

```

ax.set_xlim(0,nt*delta_t)

ax = fig.add_subplot(Nsta,Ncomp,8)
ax.plot(time_dataN3[0:nt*10],N33[0:nt*10],'blue',label='raw data')
ax.plot(time_des, seismograms[2,1,:],'red',label='interpolation')
ax.set_title('North',fontsize='14',fontweight='bold')
ax.set_xlim(0,nt*delta_t)

ax = fig.add_subplot(Nsta,Ncomp,9)
ax.plot(time_dataZ3[0:nt*10],Z33[0:nt*10],'blue',label='raw data')
ax.plot(time_des, seismograms[2,2,:],'red',label='interpolation')
ax.set_title('Vertical',fontsize='14',fontweight='bold')
ax.set_xlim(0,nt*delta_t)

# station 4 (WUPA)
ax = fig.add_subplot(Nsta,Ncomp,10)
ax.plot(time_dataE4[0:nt*10],E44[0:nt*10],'blue',label='raw data')
ax.plot(time_des, seismograms[3,0,:],'red',label='interpolation')
ax.set_title('East',fontsize='14',fontweight='bold')
ax.set_ylabel('WUPA',fontsize='14',fontweight='bold')
ax.set_xlim(0,nt*delta_t)

ax = fig.add_subplot(Nsta,Ncomp,11)
ax.plot(time_dataN4[0:nt*10],N44[0:nt*10],'blue',label='raw data')
ax.plot(time_des, seismograms[3,1,:],'red',label='interpolation')
ax.set_title('North',fontsize='14',fontweight='bold')
ax.set_xlim(0,nt*delta_t)

ax = fig.add_subplot(Nsta,Ncomp,12)
ax.plot(time_dataZ4[0:nt*10],Z44[0:nt*10],'blue',label='raw data')
ax.plot(time_des, seismograms[3,2,:],'red',label='interpolation')
ax.set_title('Vertical',fontsize='14',fontweight='bold')
ax.set_xlim(0,nt*delta_t)

# station 5 (REST)
ax = fig.add_subplot(Nsta,Ncomp,13)
ax.plot(time_dataE5[0:nt*10],E55[0:nt*10],'blue',label='raw data')
ax.plot(time_des, seismograms[4,0,:],'red',label='interpolation')
ax.set_title('East',fontsize='14',fontweight='bold')
ax.set_ylabel('REST',fontsize='14',fontweight='bold')
ax.set_xlim(0,nt*delta_t)

ax = fig.add_subplot(Nsta,Ncomp,14)
ax.plot(time_dataN5[0:nt*10],N55[0:nt*10],'blue',label='raw data')
ax.plot(time_des, seismograms[4,1,:],'red',label='interpolation')
ax.set_title('North',fontsize='14',fontweight='bold')

```

```

ax.set_xlim(0,nt*delta_t)

ax = fig.add_subplot(Nsta,Ncomp,15)
ax.plot(time_dataZ5[0:nt*10],Z55[0:nt*10],'blue',label='raw data')
ax.plot(time_des, seismograms[4,2,:],'red',label='interpolation')
ax.set_title('Vertical',fontsize='14',fontweight='bold')
ax.set_xlim(0,nt*delta_t)

# station 6 (R0ECF)
ax = fig.add_subplot(Nsta,Ncomp,16)
ax.plot(time_dataE6[0:nt*10],E66[0:nt*10],'blue',label='raw data')
ax.plot(time_des, seismograms[5,0,:],'red',label='interpolation')
ax.set_title('East',fontsize='14',fontweight='bold')
ax.set_ylabel('R0ECF',fontsize='14',fontweight='bold')
ax.set_xlim(0,nt*delta_t)

ax = fig.add_subplot(Nsta,Ncomp,17)
ax.plot(time_dataN6[0:nt*10],N66[0:nt*10],'blue',label='raw data')
ax.plot(time_des, seismograms[5,1,:],'red',label='interpolation')
ax.set_title('North',fontsize='14',fontweight='bold')
ax.set_xlim(0,nt*delta_t)

ax = fig.add_subplot(Nsta,Ncomp,18)
ax.plot(time_dataZ6[0:nt*10],Z66[0:nt*10],'blue',label='raw data')
ax.plot(time_des, seismograms[5,2,:],'red',label='interpolation')
ax.set_title('Vertical',fontsize='14',fontweight='bold')
ax.set_xlim(0,nt*delta_t)

# station 7 (RAD82)
ax = fig.add_subplot(Nsta,Ncomp,19)
ax.plot(time_dataE7[0:nt*10],E77[0:nt*10],'blue',label='raw data')
ax.plot(time_des, seismograms[6,0,:],'red',label='interpolation')
ax.set_title('East',fontsize='14',fontweight='bold')
ax.set_ylabel('RAD82',fontsize='14',fontweight='bold')
ax.set_xlim(0,nt*delta_t)

ax = fig.add_subplot(Nsta,Ncomp,20)
ax.plot(time_dataN7[0:nt*10],N77[0:nt*10],'blue',label='raw data')
ax.plot(time_des, seismograms[6,1,:],'red',label='interpolation')
ax.set_title('North',fontsize='14',fontweight='bold')
ax.set_xlim(0,nt*delta_t)

ax = fig.add_subplot(Nsta,Ncomp,21)
ax.plot(time_dataZ7[0:nt*10],Z77[0:nt*10],'blue',label='raw data')
ax.plot(time_des, seismograms[6,2,:],'red',label='interpolation')
ax.set_title('Vertical',fontsize='14',fontweight='bold')

```

```
ax.set_xlim(0,nt*delta_t)
```

```
plt.tight_layout()
```

Part 3: The Inversion

```
#####  
##### Velocity Model #####  
#####
```

```
# SE PA Velocity Model (Nyblade & Homman, 2016)  
# Calculates model parameters using P-wave relations from Brocher, 2005  
#VP = [6,6.3,6.6,6.9,8.1]  
#TH = [10,10,10,7,np.inf]
```

```
# Chapman (2013) model for Mineral, VA  
VP = [6.09,6.5,8.15]  
TH = [15,21,np.inf]  
VS = [3.53,3.79,4.73]
```

```
# Munsey and Bollinger (1985) - East of Richmond  
#VP = [6.09,6.67,8.18]  
#TH = [18,18,np.inf]  
#VS = [3.52,3.86,4.73]
```

```
lay = len(VP)
```

```
LAYERS = np.zeros(shape=(lay,4))
```

```
for i in range (lay):
```

```
    LAYERS[i,0] = TH[i] # thickness(km)  
    LAYERS[i,1] = VP[i] # v_p (km/s)  
    LAYERS[i,2] = VS[i] # v_s (km/s)  
    #LAYERS[i,2] = LAYERS[i,1]/1.74  
    #LAYERS[i,2] = 0.7858 - 1.2344*VP[i] + 0.7949*VP[i]**2 - 0.1238*VP[i]**3 +  
0.0064*VP[i]**4 # v_s (km/s)  
    LAYERS[i,3] = 1.6612*VP[i] - 0.4721*VP[i]**2 + 0.0671*VP[i]**3 - 0.0043*VP[i]**4 +  
0.000106*VP[i]**5 # density
```

```
model = pp.LayeredStructureModel(LAYERS)  
print(model)
```

```
#####
```

```

##### Station Setup #####
#####

time_orig = 0

# RECEIVER STATIONS: SDMD, SUDB, FMMC, WUPA
# [longitude, latitude]
SDMD = [-76.84033,39.41017]
SUDB = [-77.05,38.99]
FMMC = [-76.26,40.14]
WUPA = [-75.60600,39.93240]
REST = [-77.337348,38.972527]
R0ECF = [-76.654731,39.207207]
RAD82 = [-76.503509,39.594594]

#PSUB = [-75.45139,39.92739]

stations = np.array([SDMD,SUDB,FMMC,WUPA,REST,R0ECF,RAD82])

receivers = pp.ListOfReceivers(stations[:,0],stations[:,1],geometry = 'spherical')

point_force = np.zeros([3,1])

# Source position using Latitude (y) and Longitude (x)
source_x = -76.7078 # source longitude
source_y = 39.3043 # source latitude
source_depth = 9 # original 2.5

#source_time_func = lambda w: stf_trapezoidal(w, .05, .1) # not using to avoid artifacts from
convolution

#####
##### Fundamental Moment Tensors #####
#####

# Fundamental Moment Tensors

# [M11,M22,M33,M12,M13,M23]
MT11 = [1,0,0,0,0,0]
#obspy.imaging.beachball.beachball(MT11)
MT_11 = np.array([[ 1, 0, 0],
                  [ 0, 0, 0],
                  [ 0, 0, 0]])
MT22 = [0,1,0,0,0,0]
#obspy.imaging.beachball.beachball(MT22)

```

```

MT_22 = np.array([[ 0, 0, 0],
                  [ 0, 1, 0],
                  [ 0, 0, 0]])
MT33 = [0,0,1,0,0,0]
#obspy.imaging.beachball.beachball(MT33)
MT_33 = np.array([[ 0, 0, 0],
                  [ 0, 0, 0],
                  [ 0, 0, 1]])
MT12 = [0,0,0,1,0,0]
#obspy.imaging.beachball.beachball(MT12)
MT_12 = np.array([[ 0, 1, 0],
                  [ 1, 0, 0],
                  [ 0, 0, 0]])
MT13 = [0,0,0,0,1,0]
#obspy.imaging.beachball.beachball(MT13)
MT_13 = np.array([[ 0, 0, 1],
                  [ 0, 0, 0],
                  [ 1, 0, 0]])
MT23 = [0,0,0,0,0,1]
#obspy.imaging.beachball.beachball(MT23)
MT_23 = np.array([[ 0, 0, 0],
                  [ 0, 0, 1],
                  [ 0, 1, 0]])

M = np.array([MT_11,MT_22,MT_33,MT_12,MT_13,MT_23,])

#####
##### Set up Matrix Equation #####
#####

G_length = Nsta*Ncomp*nt
G = np.zeros(shape=(G_length,6))
obs_seismogram = np.zeros(shape=(G_length,1))

# Make data vector
for i in range(Nsta):
    for j in range(Ncomp):
        A = (i*(Ncomp*nt)+j*nt)
        B = (i*(Ncomp*nt)+(j+1)*nt)
        obs_seismogram[A:B:1,0] = seismograms[i,j,:]*1000;

# Compute fundamental fault type seismograms
source = pp.PointSource(source_x,source_y,source_depth,M[0],point_force,time_orig)
time,seismograms11A = pp.compute_seismograms(model, source, receivers, nt, delta_t,
                                             xyz=True,source_time_function=lambda w:stf_cosine(w,.2))

```

```

source = pp.PointSource(source_x,source_y,source_depth,M[1],point_force,time_orig)
time,seismograms22A = pp.compute_seismograms(model, source, receivers, nt, delta_t,
xyz=True,source_time_function=lambda w:stf_cosine(w,.2))

source = pp.PointSource(source_x,source_y,source_depth,M[2],point_force,time_orig)
time,seismograms33A = pp.compute_seismograms(model, source, receivers, nt, delta_t,
xyz=True,source_time_function=lambda w:stf_cosine(w,.2))

source = pp.PointSource(source_x,source_y,source_depth,M[3],point_force,time_orig)
time,seismograms12A = pp.compute_seismograms(model, source, receivers, nt, delta_t,
xyz=True,source_time_function=lambda w:stf_cosine(w,.2))

source = pp.PointSource(source_x,source_y,source_depth,M[4],point_force,time_orig)
time,seismograms13A = pp.compute_seismograms(model, source, receivers, nt, delta_t,
xyz=True,source_time_function=lambda w:stf_cosine(w,.2))

source = pp.PointSource(source_x,source_y,source_depth,M[5],point_force,time_orig)
time,seismograms23A = pp.compute_seismograms(model, source, receivers, nt, delta_t,
xyz=True,source_time_function=lambda w:stf_cosine(w,.2))

# New Filter
sos = signal.butter(4, [0.5, 1], btype='bandpass', analog=False, output='sos',fs=1/delta_t)

# Filter fundamental seismograms
seismograms11D = signal.sosfilt(sos, seismograms11A)
seismograms22D = signal.sosfilt(sos, seismograms22A)
seismograms33D = signal.sosfilt(sos, seismograms33A)
seismograms12D = signal.sosfilt(sos, seismograms12A)
seismograms13D = signal.sosfilt(sos, seismograms13A)
seismograms23D = signal.sosfilt(sos, seismograms23A)

seismograms11 = np.zeros(shape=(Nsta,Ncomp,nt))
seismograms22 = np.zeros(shape=(Nsta,Ncomp,nt))
seismograms33 = np.zeros(shape=(Nsta,Ncomp,nt))
seismograms12 = np.zeros(shape=(Nsta,Ncomp,nt))
seismograms13 = np.zeros(shape=(Nsta,Ncomp,nt))
seismograms23 = np.zeros(shape=(Nsta,Ncomp,nt))

print('shape = ',np.shape(seismograms11D))

# Take derivatives (convert displacement to velocity)
for i in range(Nsta):
    for j in range(Ncomp):
        seismograms11[i,j,:] = np.gradient(seismograms11D[i,j,:])/delta_t

```

```

seismograms22[i,j,:] = np.gradient(seismograms22D[i,j,:])/delta_t
seismograms33[i,j,:] = np.gradient(seismograms33D[i,j,:])/delta_t
seismograms12[i,j,:] = np.gradient(seismograms12D[i,j,:])/delta_t
seismograms13[i,j,:] = np.gradient(seismograms13D[i,j,:])/delta_t
seismograms23[i,j,:] = np.gradient(seismograms23D[i,j,:])/delta_t

print('done with seismograms')
print(' ')

# Fill Green's Matrix
for i in range(Nsta):
    for j in range(Ncomp):
        G[i*(Ncomp*nt)+j*nt:i*(Ncomp*nt)+(j+1)*nt,0] = seismograms11[i,j,:]
        G[i*(Ncomp*nt)+j*nt:i*(Ncomp*nt)+(j+1)*nt,1] = seismograms22[i,j,:]
        G[i*(Ncomp*nt)+j*nt:i*(Ncomp*nt)+(j+1)*nt,2] = seismograms33[i,j,:]
        G[i*(Ncomp*nt)+j*nt:i*(Ncomp*nt)+(j+1)*nt,3] = seismograms12[i,j,:]
        G[i*(Ncomp*nt)+j*nt:i*(Ncomp*nt)+(j+1)*nt,4] = seismograms13[i,j,:]
        G[i*(Ncomp*nt)+j*nt:i*(Ncomp*nt)+(j+1)*nt,5] = seismograms23[i,j,:]

# print results
print(G)
print(np.shape(G))
print(np.shape(obs_seismogram))
print(' ')

#####
##### Zero Out unused waveform sections #####
#####

sf = int(1/delta_t) # decimated sampling frequency

# start and end of waveforms used
SDMDstart = 3 #4.8
SDMDend = 11 #7.5
SUDBstart = 12 #13
SUDBend = 20 #17.5
FMMCstart = 28
FMMCend = 35 #40
WUPAstart = 34 #23
WUPAend = 42 #33
RESTstart = 18
RESTend = 24
R0ECFstart = 1
R0ECFend = 7
RAD82start = 11
RAD82end = 16

```

```
START = [SDMDstart,SUDBstart,FMMCstart,WUPAstart,RESTstart,R0ECFstart,RAD82start]
END = [SDMDend,SUDBend,FMMCend,WUPAend,RESTend,R0ECFend,RAD82end]
```

```
for i in range(Nsta):
    for j in range(Ncomp):
        obs_seismogram[i*(Ncomp*nt)+j*nt : i*(Ncomp*nt)+j*nt+sf*START[i] , 0 ] = 0
        obs_seismogram[i*(Ncomp*nt)+j*nt+sf*END[i] : i*(Ncomp*nt)+(j+1)*nt , 0] = 0

        G[i*(Ncomp*nt)+j*nt : i*(Ncomp*nt)+j*nt+sf*START[i] , : ] = 0
        G[i*(Ncomp*nt)+j*nt+sf*END[i] : i*(Ncomp*nt)+(j+1)*nt , :] = 0
```

```
# zero E and N componenets of RAD82 station with only Z data
#obs_seismogram[6*Ncomp*nt:6*Ncomp*nt+2*nt] = 0
G[6*Ncomp*nt:6*Ncomp*nt+2*nt,:] = 0
```

```
#####
##### INVERSION #####
#####
```

```
# division by 1000 necessary for units when using real data, but not with synthetic data
M,R,r,s = np.linalg.lstsq(G,obs_seismogram)
```

```
Cov_M_post = np.linalg.inv(np.matmul(np.transpose(G),G))/1e6;
print('covariance matrix = ',Cov_M_post)
print(' ')
```

```
print('Moment Tensor [11,22,33,12,13,23]')
print(M)
print(' ')
```

```
#inv = np.linalg.inv(GG)
print(np.shape(G))
print(np.shape(obs_seismogram))
```

```
# Make Beachball plot
```

```
M11 = float(M[0])
M22 = float(M[1])
M33 = float(M[2])
M12 = float(M[3])
M13 = float(M[4])
M23 = float(M[5])
```

```
MT_inversion = np.array([M33,M22,M11,-M23,M13,-M12])
```

```

print('Focal Mechanism Solution')
obspy.imaging.beachball.beachball(MT_inversion)

#Calculate Scalar Moment and Magnitude

M_0 = np.sqrt((M11)**2 + (M22)**2 + (M33)**2 + (M12)**2 + (M13)**2 +
(M23)**2)/np.sqrt(2)
print('Scalar moment = ',M_0)
print(' ')
Mw = (2/3)*(np.log10(M_0*10**12) - 9.1)
print('Mw = ', Mw)

plt.plot(np.matmul(G,M))

```

Part 4: Compare plots of data and inversion results to help assign time shifts

```

#####
##### Plot Data vs Inversion Waveforms #####
#####

print('working ...')

#Compute Variance Reduction
var_data = np.var(obs_seismogram)
var_res = np.var(obs_seismogram - np.matmul(G,M))
var_red = 1-(var_res)/var_data
print('variance reduction = ',var_red)

# Make synthetics using Inversion Moment Tensor

MT = np.array([[M11,M12,M13],
               [M12,M22,M23],
               [M13,M23,M33]])

#Decompose moment tensor and find percent Double Couple
trace = M11 + M22 + M33
MTdev = MT - np.identity(3)*trace/3
print(MTdev+np.identity(3)*trace/3)

evals,evecs = np.linalg.eig(MTdev)
print(evals)
#print(min(evals))

epsilon = abs(min(evals)) / abs(max(evals))
#print(epsilon)

```

```

source = pp.PointSource(source_x,source_y,source_depth,MT,point_force,time_orig)

time,inversion = pp.compute_seismograms(model, source, receivers, nt, delta_t,
xyz=True,source_time_function=lambda w:stf_cosine(w,.2))

inversion1 = np.zeros(shape=(Nsta,Ncomp,nt))
inversion2 = np.zeros(shape=(Nsta,Ncomp,nt))

# filter and divide by 1000 to achieve correct units
inversion1 = signal.sosfilt(sos, inversion)/1000

# Change from distance to velocity
inversion2[0,0,:] = np.gradient(inversion1[0,0,0:nt])/delta_t
inversion2[0,1,:] = np.gradient(inversion1[0,1,0:nt])/delta_t
inversion2[0,2,:] = np.gradient(inversion1[0,2,0:nt])/delta_t
inversion2[1,0,:] = np.gradient(inversion1[1,0,0:nt])/delta_t
inversion2[1,1,:] = np.gradient(inversion1[1,1,0:nt])/delta_t
inversion2[1,2,:] = np.gradient(inversion1[1,2,0:nt])/delta_t
inversion2[2,0,:] = np.gradient(inversion1[2,0,0:nt])/delta_t
inversion2[2,1,:] = np.gradient(inversion1[2,1,0:nt])/delta_t
inversion2[2,2,:] = np.gradient(inversion1[2,2,0:nt])/delta_t
inversion2[3,0,:] = np.gradient(inversion1[3,0,0:nt])/delta_t
inversion2[3,1,:] = np.gradient(inversion1[3,1,0:nt])/delta_t
inversion2[3,2,:] = np.gradient(inversion1[3,2,0:nt])/delta_t
inversion2[4,0,:] = np.gradient(inversion1[4,0,0:nt])/delta_t
inversion2[4,1,:] = np.gradient(inversion1[4,1,0:nt])/delta_t
inversion2[4,2,:] = np.gradient(inversion1[4,2,0:nt])/delta_t
inversion2[5,0,:] = np.gradient(inversion1[5,0,0:nt])/delta_t
inversion2[5,1,:] = np.gradient(inversion1[5,1,0:nt])/delta_t
inversion2[5,2,:] = np.gradient(inversion1[5,2,0:nt])/delta_t
inversion2[6,0,:] = np.gradient(inversion1[6,0,0:nt])/delta_t
inversion2[6,1,:] = np.gradient(inversion1[6,1,0:nt])/delta_t
inversion2[6,2,:] = np.gradient(inversion1[6,2,0:nt])/delta_t

fig = plt.figure(figsize=(12,3*Nsta))
#fig.suptitle('Comparison of Waveforms and Inversion for Baltimore
6/25/21',fontsize='18',fontweight='bold')

# Station 1

ax = fig.add_subplot(Nsta,Ncomp,1)
ax.plot(time,seismograms[0,0,:],'blue',label='data')
ax.plot(time,inversion2[0,0,:],'red',label='inversion')
ax.set_title('East',fontsize='14',fontweight='bold')

```

```

#ax.set_ylabel("Velocity (m/s)",fontsize='10')
ax.set_ylabel('SDMD',fontsize='14',fontweight='bold')
ax.set_xlim(0,10)
ax.legend()

ax = fig.add_subplot(Nsta,Ncomp,2)
ax.plot(time,seismograms[0,1,:],'blue',label='data')
ax.plot(time,inversion2[0,1,:],'red',label='inversion')
ax.set_title('North',fontsize='14',fontweight='bold')
ax.set_xlim(0,10)

ax = fig.add_subplot(Nsta,Ncomp,3)
ax.plot(time,seismograms[0,2,:],'blue',label='data')
ax.plot(time,inversion2[0,2,:],'red',label='inversion')
ax.set_title('Vertical',fontsize='14',fontweight='bold')
ax.set_xlim(0,10)

# Station 2

ax = fig.add_subplot(Nsta,Ncomp,4)
ax.plot(time,seismograms[1,0,:],'blue',label='data')
ax.plot(time,inversion2[1,0,:],'red',label='inversion')
#ax.set_ylabel("Velocity (m/s)",fontsize='10')
ax.set_ylabel('SUDB',fontsize='14',fontweight='bold')
ax.set_xlim(10,20)

ax = fig.add_subplot(Nsta,Ncomp,5)
ax.plot(time,seismograms[1,1,:],'blue',label='data')
ax.plot(time,inversion2[1,1,:],'red',label='inversion')
ax.set_xlim(10,20)

ax = fig.add_subplot(Nsta,Ncomp,6)
ax.plot(time,seismograms[1,2,:],'blue',label='data')
ax.plot(time,inversion2[1,2,:],'red',label='inversion')
ax.set_xlim(10,20)

# Station 3

ax = fig.add_subplot(Nsta,Ncomp,7)
ax.plot(time,seismograms[2,0,:],'blue',label='data')
ax.plot(time,inversion2[2,0,:],'red',label='inversion')
ax.set_xlabel("Time (s)",fontsize='10')
#ax.set_ylabel("Velocity (m/s)",fontsize='10')
ax.set_ylabel('FMMC',fontsize='14',fontweight='bold')
ax.set_xlim(25,35)

```

```

ax = fig.add_subplot(Nsta,Ncomp,8)
ax.plot(time,seismograms[2,1,:],'blue',label='data')
ax.plot(time,inversion2[2,1,:],'red',label='inversion')
ax.set_xlabel("Time (s)",fontsize='10')
ax.set_xlim(25,35)

ax = fig.add_subplot(Nsta,Ncomp,9)
ax.plot(time,seismograms[2,2,:],'blue',label='data')
ax.plot(time,inversion2[2,2,:],'red',label='inversion')
ax.set_xlabel("Time (s)",fontsize='10')
ax.set_xlim(25,35)

# Station 4

ax = fig.add_subplot(Nsta,Ncomp,10)
ax.plot(time,seismograms[3,0,:],'blue',label='data')
ax.plot(time,inversion2[3,0,:],'red',label='inversion')
ax.set_xlabel("Time (s)",fontsize='10')
#ax.set_ylabel("Velocity (m/s)",fontsize='10')
ax.set_ylabel('WUPA',fontsize='14',fontweight='bold')
ax.set_xlim(30,42)

ax = fig.add_subplot(Nsta,Ncomp,11)
ax.plot(time,seismograms[3,1,:],'blue',label='data')
ax.plot(time,inversion2[3,1,:],'red',label='inversion')
ax.set_xlabel("Time (s)",fontsize='10')
ax.set_xlim(30,42)

ax = fig.add_subplot(Nsta,Ncomp,12)
ax.plot(time,seismograms[3,2,:],'blue',label='data')
ax.plot(time,inversion2[3,2,:],'red',label='inversion')
ax.set_xlabel("Time (s)",fontsize='10')
ax.set_xlim(30,42)

# Station 5

ax = fig.add_subplot(Nsta,Ncomp,13)
ax.plot(time,seismograms[4,0,:],'blue',label='data')
ax.plot(time,inversion2[4,0,:],'red',label='inversion')
ax.set_xlabel("Time (s)",fontsize='10')
#ax.set_ylabel("Velocity (m/s)",fontsize='10')
ax.set_ylabel('REST',fontsize='14',fontweight='bold')
ax.set_xlim(15,30)

ax = fig.add_subplot(Nsta,Ncomp,14)
ax.plot(time,seismograms[4,1,:],'blue',label='data')

```

```

ax.plot(time,inversion2[4,1,:],'red',label='inversion')
ax.set_xlabel("Time (s)",fontsize='10')
ax.set_xlim(15,30)

```

```

ax = fig.add_subplot(Nsta,Ncomp,15)
ax.plot(time,seismograms[4,2,:],'blue',label='data')
ax.plot(time,inversion2[4,2,:],'red',label='inversion')
ax.set_xlabel("Time (s)",fontsize='10')
ax.set_xlim(15,30)

```

Station 6

```

ax = fig.add_subplot(Nsta,Ncomp,16)
ax.plot(time,seismograms[5,0,:],'blue',label='data')
ax.plot(time,inversion2[5,0,:],'red',label='inversion')
ax.set_xlabel("Time (s)",fontsize='10')
#ax.set_ylabel("Velocity (m/s)",fontsize='10')
ax.set_ylabel('R0ECF',fontsize='14',fontweight='bold')
ax.set_xlim(0,15)

```

```

ax = fig.add_subplot(Nsta,Ncomp,17)
ax.plot(time,seismograms[5,1,:],'blue',label='data')
ax.plot(time,inversion2[5,1,:],'red',label='inversion')
ax.set_xlabel("Time (s)",fontsize='10')
ax.set_xlim(0,15)

```

```

ax = fig.add_subplot(Nsta,Ncomp,18)
ax.plot(time,seismograms[5,2,:],'blue',label='data')
ax.plot(time,inversion2[5,2,:],'red',label='inversion')
ax.set_xlabel("Time (s)",fontsize='10')
ax.set_xlim(0,15)

```

Station 7

No E and N channels

```

ax = fig.add_subplot(Nsta,Ncomp,21)
ax.plot(time,seismograms[6,2,:],'blue',label='data')
ax.plot(time,inversion2[6,2,:],'red',label='inversion')
ax.set_xlabel("Time (s)",fontsize='10')
ax.set_xlim(5,20)
ax.set_ylabel('RAD82',fontsize='14',fontweight='bold')

```

```

plt.tight_layout()

```

```

plt.savefig('Chapman model waveforms')

```

Part 5: Decompose Moment Tensor and Plot Focal Mechanisms

```
import pyrocko
from pyrocko import moment_tensor as pmt
from pyrocko import util

from pyrocko.plot import beachball

r2d = 180. / np.pi

exp = 1e12

#init pyrocko moment tensor
# input moment tensor and covert from ENU to NED
m = pmt.MomentTensor(
    mnn=M22*exp,
    mee=M11*exp,
    mdd=M33*exp,
    mne=M12*exp,
    mnd=-M23*exp,
    med=-M13*exp)
# init pyrocko moment tensor
#m = pmt.MomentTensor(M11*exp, M22*exp, M33*exp,M12*exp,M13*exp,M23*exp)

print(m)

# gives out both nodal planes:
(s1, d1, r1), (s2, d2, r2) = m.both_strike_dip_rake()

print('strike1=%g, dip1=%g, rake1=%g' % (s1, d1, r1))
print('strike2=%g, dip2=%g, rake2=%g' % (s2, d2, r2))

# p-axis normal vector in north-east-down coordinates
p_ned = m.p_axis()

print('p_ned=(%g, %g, %g)' % tuple(p_ned))

# convert to azimuth and dip
p_azimuth = np.arctan2(p_ned[1], p_ned[0]) * r2d
p_dip = np.arcsin(p_ned[2]) * r2d

print('p_azimuth=%g, p_dip=%g' % (p_azimuth, p_dip))

fig = plt.figure(figsize=(8., 4.))
```

```

fig.subplots_adjust(left=-1, right=1, bottom=-1, top=1)
axes = fig.add_subplot(1, 1, 1)

beachball.plot_beachball_mpl(m, axes, beachball_type='full',
                             position=(0.25, 0.5), size=400, zorder=0,
                             color_t=(.99, .9, .9), color_p='white', edgecolor='black',
                             linewidth=2, alpha=1.0, arcres=181, decimation=1,
                             projection='lambert', size_units='points', view='top')
beachball.plot_beachball_mpl(m, axes, beachball_type='dc',
                             position=(0.75, 0.5), size=400, zorder=0,
                             color_t='red', color_p='white', edgecolor='black',
                             linewidth=2, alpha=1.0, arcres=181, decimation=1,
                             projection='lambert', size_units='points', view='top')

#print(pmt.standard_decomposition(m))
DECOMP = pmt.MomentTensor.standard_decomposition(m)
iso = DECOMP[0][2]
DC = DECOMP[1][2]
CLVD = DECOMP[2][2]
print(DC)

# tension axis
T = pmt.MomentTensor.t_axis(m)
print(T)
pmt.ned_to_rta(T)

```

Part 6: Find maximum moment tensor angle

```

#####
##### Compute angle between moment tensors #####
#####
import numpy as np
import matplotlib.pyplot as plt

MT1 = np.array([11.26594625, 16.07641646, 1.0722181, 9.94899155, 11.52840342,
5.99694943])

MT2 = np.array([13.28192687, 14.06307988, 1.62255055, 11.69378714, 10.70946245,
6.56679103])

MT3 = np.array([12.7352061, 17.01967496, 1.55145649, 11.19032123, 12.21622611,
6.47134821])

MT4 = np.array([16.3378397, 17.80915232, 0.48315376, 13.84689468, 13.57120277,
9.12144183])

```

```

MTS = np.array([MT1, MT2, MT3, MT4])

for i in range(4):
    MTi = MTS[i]
    for j in range(4):
        MTj = MTS[j]
        a = MTi[0]; b = MTi[1]; c = MTi[2]; d = MTi[3]; e = MTi[4]; f = MTi[5];
        aa = MTj[0]; bb = MTj[1]; cc = MTj[2]; dd = MTj[3]; ee = MTj[4]; ff = MTj[5];

        # angle between measured and true moment tensor (measure of misfit)
        # normalized so max angular misfit is 1, min = 0
        dotproduct = a*aa + b*bb + c*cc + d*dd + e*ee + f*ff
        norm1 = np.sqrt(a*a + b*b + c*c + d*d + e*e + f*f)
        norm2 = np.sqrt(aa*aa + bb*bb + cc*cc + dd*dd + ee*ee + ff*ff)
        MT_angle = np.arccos( dotproduct / (norm1 * norm2) ) / np.pi
        print('Moment Tensor Angle = ', MT_angle)

```

Part 7: Plot all moment tensors on Hudson Plot

```

import pyrocko
from pyrocko import moment_tensor as pmt
from pyrocko import util
from pyrocko.plot import hudson, beachball, mpl_init, mpl_color

```

```

r2d = 180. / np.pi

```

```

magnitude = 6.3 # Magnitude of the earthquake

```

```

exp = 1e12

```

```

# setup plot layout
fontsize = 10.
markersize = fontsize
mpl_init(fontsize=fontsize)
width = 5.
figsize = (width, width / (4. / 3))
fig = plt.figure(figsize=figsize)
axes = fig.add_subplot(1, 1, 1)
fig.subplots_adjust(left=0.03, right=0.97, bottom=0.03, top=0.97)

```

```

colors = ['red','green','blue','magenta']

```

```

for i in range(4):

```

```

MTi = MTS[i]
# input moment tensor and covert from ENU to NED
m = pmt.MomentTensor(
    mnn=MTi[1]*exp,
    mee=MTi[0]*exp,
    mdd=MTi[2]*exp,
    mne=MTi[3]*exp,
    mnd=-MTi[5]*exp,
    med=-MTi[4]*exp)
# init pyrocko moment tensor
#m = pmt.MomentTensor(M11*exp, M22*exp, M33*exp,M12*exp,M13*exp,M23*exp)

# draw focal sphere diagrams for the random MTs
u, v = hudson.project(m)
try:
    beachball.plot_beachball_mpl(
        m, axes,
        beachball_type='full',
        position=(u, v),
        size=markersize,
        #color_t=mpl_color('skyblue3'),
        color_t=mpl_color(colors[i]),
        #color_p=mpl_color('skyblue1'),
        color_p=mpl_color(colors[i]),
        alpha=1.0, # < 1 for transparency
        zorder=1,
        linewidth=0.25)

except beachball.BeachballError as e:
    print(str(e), file=sys.stderr)

# draw the axes and annotations of the hudson plot
hudson.draw_axes(axes)

#fig.savefig('hudson_diagram.png', dpi=150)
# plt.show()

```